Mon. Not. R. Astron. Soc. **000**, 1–56 (2002) Printed 5 February 2008 (MN LaTeX style file v2.2)

arXiv:astro-ph/0512150v1 6 Dec 2005

Dynamic tides in rotating objects: orbital circularisation of extra solar planets for realistic planet models

P. B. Ivanov[1,2]⋆ and J. C. B. Papaloizou[1] ⋆

[1] *Department of Applied Mathematics and Theoretical Physics, University of Cambridge,*
Centre for Mathematical Sciences, Wilberforce Road, Cambridge, CB3 0WA, UK

[2] *Astro Space Centre, P. N. Lebedev Physical Institute, 4/32 Profsoyuznaya Street, Moscow, 117810, Russia*

Accepted Received ; in original form

ABSTRACT

We consider the general problem of the tidal capture or circularisation from large eccentricity of a uniformly rotating object. We extend the self-adjoint formalism introduced in our recent paper(Papaloizou & Ivanov 2005 hereafter PI)) to derive general expressions for the energy and angular momentum transfered when the planet or a star passes through periastron in a parabolic or highly eccentric orbit around a central mass. These can be used without making a low frequency approximation as was done in PI. We show how these can be adapted to the low frequency limit in which only inertial modes contribute for baratropic planet models. In order to make quantitative estimates, we calculate the inertial mode eigenspectrum for planet models of one and five Jupiter masses M_J, without a solid core, with different radii corresponding to different ages. The spectra are found in general to be more complex than of a polytrope with index $n = 1.5$, considered in PI, because of the existence global modes associated with the transition from molecular to metallic Hydrogen. Nonetheless the main tidal response is still found to be determined by two global modes which have polytropic counterparts.

These also determine the uniform angular velocity in a state of pseudo synchronisation, for which the angular momentum transfered during an encounter is zero. This is found to be close to 1.55 times the circular orbit angular velocity at periastron for all models considered. This is in contrast to

© 2002 RAS

the situation when only the f mode is considered (Ivanov & Papaloizou 2004, hereafter IP) and the equilibrium angular velocity is found to be much larger.

We consider the multi-passage problem when there is no dissipation finding that stochastic instability resulting in the stochastic gain of inertial mode energy over many periastron passages occurs under similar conditions to those already found by IP for the f modes. We find that this requires circularisation to start with a semi-major axis exceeding $\sim 30AU$, for final periods of ~ 3 days. reducing to $\sim 1-2AU$ for final periods ~ 1.2 days.

Finally we apply our calculations of the energy transfer during a periastron passage to the problem of the tidal circularisation of the orbits of the extrasolar planets in a state of pseudo synchronisation, expected because of the relatively small inertia of the planet, and find that inertial mode excitation dominates the tidal interaction for $1M_J$ planets that start with semi- major axes less than $10AU$ and end up on circular orbits with final period in the $4-6$ day range. It is potentially able to account for initial circularisation up to a final 6 day period within a few Gyr But in the case of $5M_J$ oscillation modes excited in the star are more important.

Key words: hydrodynamics; stars: oscillations, binaries, rotation; planetary systems: formation

1 INTRODUCTION

The process of tidal capture, whereby a body in initially unbound orbit has a close approach to another gravitating mass, and through the excitation of internal modes of oscillation, becomes subsequently bound is of general importance in astrophysics. It is believed to play a role in binary formation in globular clusters (eg. Press & Teukolsky 1977, hereafter PT, and references therein) and to play a role in the tidal interactions of stars in galactic centres. A related problem is the circularisation of an orbit from large eccentricity which may occur after a tidal capture. In this situation, each periastron passage is very similar to a close encounter in a weakly unbound orbit that causes a change in the energy contained within internal modes of oscillation at the expense of that in the orbit.

In order to estimate capture probabilities and circularisation time scales the excitation of normal modes of oscillation by a perturbing potential must be considered. In general modes associated with spherical stars, or small perturbations of them, have been considered (eg. PT, IP and references therein). However, if the tidally perturbed body has multiple encounters,

---

[*] E-mail:P.Ivanov@damtp.cam.ac.uk (PBI) J.C.B.Papaloizou@damtp.cam.ac.uk (JCBP)

angular momentum transfer should lead it to rotate at an angular velocity related to that at periastron. In this case modes of oscillation with periods comparable to the rotation period need to be considered (eg. Papaloizou & Pringle 1978).

An approach for dealing with the problem of calculating tidal phenomena while taking into account the part of the oscillation spectrum with eigen frequencies comparable to the rotation frequency was recently proposed by PI. They adopted a self-adjoint formalism for calculating the tidal response that used the density perturbation to describe the motions within the star and they made a low frequency approximation that the rotation and mode frequencies were very much less than the inverse sound crossing time. They also evaluated the inertial mode spectrum for a polytrope with index $n = 3/2$ and showed that inertial modes dominated the response at low frequencies or large periastron distances.

Given the importance of rotation, the purpose of this paper is to develop further the work begun in PI and to use the results to obtain time scales for tidal phenomena such as circularisation of the orbit starting from high eccentricity.

We begin by noting that the self-adjoint formalism can be extended to general linear displacements without making a low frequency approximation. In this form, which uses the Lagrangian displacement to describe the perturbations it has wider applicability than the formalism presented in PI which made a low frequency approximation. We also wish to evaluate the expressions obtained for the energy and angular momentum exchanged during close periastron passages for realistic planet models. Accordingly we calculate sequences of models of one Jupiter mass M_J and $5M_J$. Each sequence has a range of radii in order to take account of the fact that the planet radius varies with age. For simplicity we do not include a solid core noting that according to Saumon & Guillot (2004) observations of Jupiter are not inconsistent with this. We calculate the oscillation spectra together with required overlap integrals for the models using a set of basis or trial functions.

We then use the determined eigenmode properties for these models to estimate tidal phenomena such as the attainment of pseudo synchronism for which the angular momentum transfer at periastron passage is zero. Such a state is expected to be attained, on account of the small inertia of the planet compared to that of the orbit, with subsequent energy exchanges occurring with the planet rotating at an equilibrium angular velocity. The inclusion of inertial modes is important for determining this angular velocity which turns out to be close to that of the orbit at periastron. Calculations in IP incorporating only the f modes gave a much higher value.

Having calculated the equilibrium angular velocity we are able to consider multiple encounters and determine conditions for the onset of stochastic instability, that results in the stochastic gain of inertial mode energy over many periastron passages when there is no dissipation (Kochanek 1992, Mardling 1994a,b). Then we make estimates of circularisation time scales for the two different planet masses taking into account the evolutionary variation of the planet radius with age.

The plan of the paper is as follows. In section 2 we formulate the new self-adjoint formalism for the problem of linear perturbations proposed in our recent paper(PI) using the Lagrangian displacement to describe the motions and then use it to derive general expressions for the energy and angular momentum transfered when a rotating planet or a star passes through periastron in a parabolic or highly eccentric orbit around a central mass without making a low frequency approximation as in PI. It can thus be applied to general situations in which p, f, g and inertial modes are significant. In section 3 we show that the general formalism can be reduced to that of PI in an appropriate low frequency limit. In this case only the inertial modes contribute to the tidal response for the baratropic stellar models we consider. In section 4 we discuss the tidal energy and angular momentum transfered through inertial modes giving very simple expressions that apply when the planet or star rotates in a state of pseudo synchronisation for which the angular momentum transfered in an encounter is essentially zero. We apply these to the multi-passage problem when there is no dissipation finding conditions for the occurrence of the stochastic instability. We find that this requires the circularisation process to start with a rather large semi-major axis $\sim 30AU$, for final periods of ~ 3 days. However, this could be reduced to $\sim 1-2AU$ for the shortest observed final periods ~ 1.2 days.

In section 5 we calculate the eigenspectrum of the inertial modes for the planet models which have been obtained using a realistic equation of state. We find that the counterparts of the two global modes found in a polytrope with $n = 1.5$ exist in these cases but that there are additional global modes associated with the transition from molecular to metallic Hydrogen. We go on to apply the results to the problem of tidal circularisation of the orbits of the extrasolar planets in sections 6 and 7 finding that inertial modes dominate the tidal interaction for M_J planets ending up on circular orbits with final period in the $4-6$ day range and are potentially able to account for the initial circularisation at a 6 day period within a few Gyr in that case. However, in the case of $5M_J$ oscillation modes excited in the star become more important. Finally in section 8 we discuss our results.

2 FORMAL SOLUTION OF THE TIDAL PROBLEM

In this Section we further develop the self adjoint formalism describing the pulsations of a uniformly rotating fully convective object (a planet or a star), referred to hereafter as a planet, introduced in our previous Paper (Papaloizou & Ivanov 2005, PI). We give general expressions for the energy and angular momentum transfer from the orbit to the planet as a result of a close encounter or fly by around a gravitating centre. Here, contrary to PI, we do not make the assumption that only low frequency modes respond effectively to the tidal forcing and the results obtained are valid for the excitation of any pulsational mode of a rotating planet.

The fundamental quantity used in our analysis is the Lagrangian displacement vector $\boldsymbol{\xi}$. By definition, this is real. We adopt a cylindrical coordinate system (ϖ, ϕ, z) with origin at the centre of mass of the planet.

We make use of the Fourier transforms of the displacement vector and any other perturbation quantity, say Q, over the azimuthal angle ϕ and time t in the form

$$Q = \sum_m \left(\exp(im\phi) \int_{-\infty}^{+\infty} d\sigma \tilde{Q}_m \exp(-i\sigma t) + cc \right), \qquad (1)$$

where the sum is over $m = 0$ and 2 and cc denotes the complex conjugate. The reality of Q implies that the Fourier transform, indicated by tilde satisfies $\tilde{Q}_m(\sigma) = \tilde{Q}^*_{-m}(-\sigma)$.

The inner products of two complex scalars Y_1, Y_2, and vectors $\boldsymbol{\eta}_1$ and $\boldsymbol{\eta}_2$ are defined as

$$(Y_1|Y_2) = \int \varpi d\varpi dz \rho (Y_1^* Y_2) \quad (\boldsymbol{\eta}_1|\boldsymbol{\eta}_2) = \int \varpi d\varpi dz \rho (\boldsymbol{\eta}_1^* \cdot \boldsymbol{\eta}_2), \qquad (2)$$

where $(\boldsymbol{\eta}^* \cdot \boldsymbol{\mu})$ is the scalar product, ρ is the density, and $*$ stands for the complex conjugate.

2.1 Perturbed equations of motion

We assume that, viewed from an inertial frame, the planet is rotating with uniform angular velocity $\boldsymbol{\Omega}$ directed perpendicular to the orbital plane. In this situation the hydrodynamic equations for the perturbed quantities take the simplest form in the rotating frame which we accordingly adopt.

Since the planet is fully convective, the entropy per unit of mass of the planetary gas remains approximately the same over the volume of the planet [1], and the pressure P can be considered as a function of density ρ only, $P = P(\rho)$. A perturbation of the planet may be considered as adiabatic, and therefore the same functional dependence $P = P(\rho)$ holds during perturbation as well. This condition is often referred to as the baratropic condition. In the baratropic approximation the linearised Navier-Stokes equations take the form (see PI)

---

[1] Note that this condition can be broken at the radius corresponding to phase transition of hydrogen from metallic to molecular form, see below.

$$\frac{D^2\boldsymbol{\xi}}{Dt^2} + 2\boldsymbol{\Omega} \times \frac{D\boldsymbol{\xi}}{Dt} = -\nabla W - \boldsymbol{f}_{\nu}, \tag{3}$$

where

$$W = c_s^2\rho^{'}/\rho + \Psi^{int} + \Psi^{ext}, \tag{4}$$

$\rho^{'}$ is the density perturbation, c_s is the adiabatic sound speed, Ψ^{int} is the stellar gravitational potential arising from the perturbations and Ψ^{ext} is the external forcing tidal potential. The viscous force per unit of mass is $\boldsymbol{f}_{\nu}$. In Cartesian coordinates it can be written in component form as

$$f_{\nu}^{\alpha} = -(1/\rho)t^{\alpha,\beta}_{,\beta} = (1/\rho)\{\rho\nu(\dot{\xi}^{\alpha}_{,\beta} + \dot{\xi}^{\beta}_{,\alpha} - \frac{2}{3}\dot{\xi}^{\gamma}_{,\gamma}\delta^{\beta}_{\alpha})\}_{,\beta}, \tag{5}$$

where the comma denotes differentiation and ν is the kinematic viscosity. The Greek indices enumerate spatial coordinate directions and the usual summation convention over these is adopted.

Note that the centrifugal term is absent in equation (3) being formally incorporated into the potential governing the static equilibrium of the unperturbed star. The convective derivative $\frac{D}{Dt} \equiv \frac{\partial}{\partial t}$ as there is no unperturbed motion in the rotating frame.

The linearised continuity equation is

$$\rho^{'} = -\nabla \cdot (\rho\boldsymbol{\xi}), \tag{6}$$

and the linearised Poisson equation is

$$\Delta\Psi^{int} = 4\pi G\rho^{'}. \tag{7}$$

Provided that expressions for the density, sound speed and kinematic viscosity are specified in some unperturbed model of the planet, the set of equations $(3 - 7)$ is complete. Without the viscous term on the right hand side of equation (3) these equations coincide with the analogous equations used by PI.

The perturbed potential Ψ^{int} can be formally expressed in terms of the density perturbation with help of the inverse of the Laplace operator, Δ^{-1}, and the density perturbation is expressed in terms of the displacement vector with help of the continuity equation. We have

$$\Psi^{int} = -4\pi G \Delta^{-1} \nabla \cdot (\rho \boldsymbol{\xi}). \tag{8}$$

Now we express W in terms of $\boldsymbol{\xi}$ with help of equations (4), (6) and (8). We substitute the result into equation (3) thus obtaining an equation containing only the displacement vector $\boldsymbol{\xi}$ as a dynamical variable. After making Fourier transform of this equation we get

$$\sigma^2 \tilde{\boldsymbol{\xi}}_m - \sigma \boldsymbol{\mathcal{B}} \tilde{\boldsymbol{\xi}}_m - \boldsymbol{\mathcal{C}} \tilde{\boldsymbol{\xi}}_m - \boldsymbol{f}_\nu (\tilde{\boldsymbol{\xi}}_m) = \tilde{\boldsymbol{S}}_m, \tag{9}$$

where the operators $\boldsymbol{\mathcal{B}}$ and $\boldsymbol{\mathcal{C}}$ are defined through their action on the vector $\boldsymbol{\xi}$ as

$$\boldsymbol{\mathcal{B}} \boldsymbol{\xi} = -2i \boldsymbol{\Omega} \times \boldsymbol{\xi}, \tag{10}$$

and

$$\boldsymbol{\mathcal{C}} \boldsymbol{\xi} = -\nabla ((\frac{c_s^2}{\rho} + 4\pi G \Delta^{-1}) \nabla \cdot (\rho \boldsymbol{\xi})) \tag{11}$$

It can be easily checked that the so defined operators $\boldsymbol{\mathcal{B}}$ and $\boldsymbol{\mathcal{C}}$ are self adjoint in the sense of the normal product (2). Also for the models we consider with weak self-gravity, the operator $\boldsymbol{\mathcal{C}}$ may be taken to be positive definite for displacements with a non zero density perturbation somewhere and non negative for arbitrary displacements including those with zero density perturbation everywhere.

The source term $\tilde{\boldsymbol{S}}_m$ is determined by the external forcing potential

$$\tilde{\boldsymbol{S}}_m = \nabla \tilde{\Psi}^{ext}_m. \tag{12}$$

2.2 Self adjoint form of the perturbed equation of motion and its formal solution

The presence of the viscous force $\boldsymbol{f}_\nu$ leads to dissipation of energy of the perturbed motion on a dissipation time scale. For global disturbances in astrophysical systems this time scale is typically very large compared to a time scale characterising the tidal forcing. In this situation we can treat the action of the viscous force as a perturbation.

Neglecting the contribution of the viscous term, we see equation (9) has an analogous form to one discussed by PI for low frequency perturbations. There it was shown that this form led to a standard type of eigen value problem associated with a new self adjoint operator $\boldsymbol{\mathcal{H}}$. In order to bring equation (9) to this standard type, let us formally consider the square root of the operator $\boldsymbol{\mathcal{C}}$, $\boldsymbol{\mathcal{C}}^{1/2}$, defined by the condition: $\boldsymbol{\mathcal{C}} = \boldsymbol{\mathcal{C}}^{1/2} \boldsymbol{\mathcal{C}}^{1/2}$ This can be done on account of the non negativity of $\boldsymbol{\mathcal{C}}$. Further, let us introduce a six dimensional vector $\vec{Z}$ with components

$$\boldsymbol{Z}_1 = \sigma\tilde{\boldsymbol{\xi}}_m, \quad \boldsymbol{Z}_2 = \boldsymbol{\mathcal{C}}^{1/2}\tilde{\boldsymbol{\xi}}_m. \tag{13}$$

It follows from equation (9) that the eigenvalue problem can be written in the standard form

$$\sigma\vec{Z} = \boldsymbol{\mathcal{H}}\vec{Z} + \vec{S}, \tag{14}$$

where the operator $\boldsymbol{\mathcal{H}}$ has a matrix structure

$$\boldsymbol{\mathcal{H}} = \begin{pmatrix} \boldsymbol{\mathcal{B}} & \boldsymbol{\mathcal{C}}^{1/2} \\ \boldsymbol{\mathcal{C}}^{1/2} & 0 \end{pmatrix}, \tag{15}$$

and the source six dimensional vector $\vec{S}$ has the components

$$\boldsymbol{S}_1 = \tilde{\boldsymbol{S}}_m, \quad \boldsymbol{S}_2 = 0. \tag{16}$$

It follows from equation (15) that the operator $\boldsymbol{\mathcal{H}}$ has the required self adjoint form. Now we can look for solution to equation (14) in the form:

$$\vec{Z} = \sum_k \alpha_k \vec{Z}^k, \tag{17}$$

where $\vec{Z}_k$ are the eigenfunctions of $\boldsymbol{\mathcal{H}}$ which satisfy

$$\sigma_k \vec{Z}^k = \boldsymbol{\mathcal{H}}\vec{Z}^k. \tag{18}$$

The eigen frequencies σ_k are necessarily real. Equation (18) is equivalent to equation (9) with the source term $\tilde{\boldsymbol{S}}_m = 0$.

Note that the eigen spectrum of $\boldsymbol{\mathcal{H}}$ or a part of it can be continuous. It this case the summation in (18) must be replaced by integration with an appropriate measure.

The eigen functions $\vec{Z}^k$ are orthogonal in the sense of the inner product

$$< \vec{Z}^k|\vec{Z}^l >= (\boldsymbol{Z}_1^k|\boldsymbol{Z}_1^l) + (\boldsymbol{Z}_2^k|\boldsymbol{Z}_2^l) = \sigma_k\sigma_l(\boldsymbol{\xi}_k|\boldsymbol{\xi}_l) + (\boldsymbol{\xi}_k|\boldsymbol{\mathcal{C}}\boldsymbol{\xi}_l), \tag{19}$$

where $\boldsymbol{\xi}_k = \boldsymbol{Z}_1^k/\sigma_k$

Substituting (17) into equation (14) and using (19) we obtain

$$\alpha_k = \frac{< \vec{Z}_k|\vec{S} >}{N_k(\sigma + i\sigma_\nu - \sigma_k)} = \frac{\sigma_k^2 S_k}{N_k(\sigma + i\sigma_\nu - \sigma_k)}, \tag{20}$$

where we add a small imaginary part to the frequency σ with $\sigma_\nu > 0$ in potentially resonant denominators to account for dissipation. As we show below, for modes for which the effect of viscosity can be treated as a small perturbation, an explicit expression for σ_ν can be obtained by taking into account the dissipation determined by the viscous force $\boldsymbol{f}_\nu$.

$$N_k =< \vec{Z}_k|\vec{Z}_k >= \sigma_k^2(\boldsymbol{\xi}_k|\boldsymbol{\xi}_k) + (\boldsymbol{\xi}_k|\boldsymbol{\mathcal{C}}\boldsymbol{\xi}_k) \tag{21}$$

is the norm.

The coefficients S_k determine decomposition of the source vector over the eigen functions,

$$\tilde{\boldsymbol{S}}_m = \sum_k \frac{<\vec{Z}_k|\vec{S}>}{N_k}\boldsymbol{Z}_1 = \sum_k \frac{\sigma_k^2 S_k}{N_k}\boldsymbol{\xi}_k, \qquad (22)$$

where summation is performed over all modes with a particular value of m. They can be written in the form

$$S_k = (\boldsymbol{\xi}_k|\tilde{\boldsymbol{S}}_m) = (\rho_k^{'}|\tilde{\Psi}_m^{ext}), \qquad (23)$$

where ρ_k' is the density perturbation associated with the eigenvector $\boldsymbol{\xi}_k$: $\rho_k' = -\nabla\rho\boldsymbol{\xi}_k$, and to obtain the last equality, we integrate by parts.

It is important to note that the coefficients S_k, the eigen frequencies σ_k and the associated displacement vector $\tilde{\boldsymbol{\xi}}_k$ obey a certain identity relation

$$0 = \sum_k \frac{\sigma_k S_k}{N_k}\boldsymbol{\xi}_k, \qquad (24)$$

which follows from equations (13), (22) and the orthogonality relation (19) for the eigen vectors. This relation is also required to ensure that $\tilde{\boldsymbol{\xi}}_m$ remains bounded as $\sigma \to 0$ (see below).

The solution for the displacement vector $\tilde{\boldsymbol{\xi}}_m$ follows from equations (13), (17) and (20)

$$\tilde{\boldsymbol{\xi}}_m = \sum_k \frac{\sigma_k^2 S_k}{N_k\sigma(\sigma + i\sigma_\nu - \sigma_k)}\boldsymbol{\xi}_k = \sum_k \frac{\sigma_k S_k}{N_k(\sigma + i\sigma_\nu - \sigma_k)}\boldsymbol{\xi}_k, \qquad (25)$$

where we use the relation (24) to obtain the last equality.

The displacement vector $\boldsymbol{\xi}$ is obtained from its Fourier's transform $\tilde{\boldsymbol{\xi}}_m$ by integration over σ and summation over m

$$\boldsymbol{\xi} = \sum_{m,k}\int d\sigma\{\frac{\sigma_k S_k}{N_k(\sigma + i\sigma_\nu - \sigma_k)}\boldsymbol{\xi}_k e^{-i\sigma t}e^{im\phi} + c.c.\}. \qquad (26)$$

This expression can be simplified in the limit $t \to \infty$ at which only the poles in the expression in the braces contribute significantly to the integral over σ. In this limit we may, therefore, write

$$\boldsymbol{\xi} = 2\pi i\sum_{m,k}(\frac{\sigma_k S_k}{N_k}e^{-\sigma_\nu t - i\sigma_k t}e^{im\phi}\boldsymbol{\xi}_k + c.c.). \qquad (27)$$

2.3 Energy and angular momentum transfer

It can be easily shown from equation (3) or equation (9) that the expression for the canonical energy of the perturbations is given by

$$E_c = \int_V d^3x\rho\frac{1}{2}(\dot{\boldsymbol{\xi}}^2 + \boldsymbol{\xi}\cdot\boldsymbol{\mathcal{C}}\boldsymbol{\xi}) = \pi\sum_m\{(\dot{\boldsymbol{\xi}}_m|\dot{\boldsymbol{\xi}}_m) + (\boldsymbol{\xi}_m|\boldsymbol{\mathcal{C}}\boldsymbol{\xi}_m)\}, \qquad (28)$$

where we integrate over the volume of the planet.

We evaluate the expression (28) after a close encounter, $t > 0$. Assuming that the time after closest approach is much larger than the characteristic time scale of the encounter, but nevertheless much smaller than the characteristic viscous time scale $\sim 1/\sigma_{\nu}$, we can use equation (27) setting $\sigma_{\nu} = 0$. Substituting the expression for $\boldsymbol{\xi}$ and its time derivative into (28) and taking into account equation (21) we get

$$E_c = 8\pi^3 \sum_{m,k} \frac{\sigma_k^2 S_k S_k^*}{N_k}, \tag{29}$$

where we use the orthogonality relation (19) and the expression for the norm (19).

The rate of viscous dissipation of energy is given by the standard expression

$$\dot{E}_{\nu} = \int_V d^3x \rho \nu \{ \dot{\xi}^{\alpha}_{,\beta} (\xi^{\alpha}_{,\beta} + \xi^{\beta}_{,\alpha}) - \frac{2}{3} (\dot{\xi}^{\alpha}_{,\alpha})^2 \}. \tag{30}$$

An explicit expression for the amount of energy dissipated by viscosity after the fly by, $\Delta E_{\nu} = \int_{-\infty}^{+\infty} dt \dot{E}_{\nu}$, can be obtained from (30) substituting (26) into (30) and integrating over time the resulting expression. We have

$$\Delta E_{\nu} = 8\pi^2 \int d\sigma \sigma^2 \sum_{m,k,l} \frac{\sigma_k \sigma_l S_k}{N_k N_l (\sigma - \sigma_k + i\sigma_{\nu})(\sigma - \sigma_l - i\sigma_{\nu})} S_k S_l^* a_{k,l}, \tag{31}$$

where we use the well known relation $\int dt e^{i(\sigma - \sigma^{'})} = 2\pi \delta(\sigma - \sigma^{'})$, and

$$a_{k,l} = \int \varpi d\varpi dz \{ \xi^{\alpha}_{\beta,k} ((\xi^{\alpha}_{\beta,l})^* + (\xi^{\beta}_{\alpha,l})^*) - \frac{2}{3} \xi^{\alpha}_{\alpha,k} (\xi^{\beta}_{\beta,l})^* \}. \tag{32}$$

As we have mentioned above, we assume that viscosity is very small, and the imaginary part of the frequency is much smaller than the corresponding real part. In this case, one can see from equation (31) that the leading contribution to ΔE_{ν} is determined by diagonal terms in the summation series with $k = l$. Also, only a part of the integral over σ very close to the resonance, $\sigma \sim \sigma_k$, gives a significant contribution. We obtain

$$\Delta E_{\nu} = 8\pi^2 \sum_{m,k} \frac{\sigma_k^4 S_k S_k^*}{N_k^2} a_{k,k} \int \left(\frac{d\sigma}{(\sigma - \sigma_k)^2 + \sigma_{\nu}^2} \right) = \frac{8\pi^3}{\sigma_{\nu}} \sum_{m,k} \frac{\sigma_k^4 S_k S_k^*}{N_k^2} a_{k,k}. \tag{33}$$

The amount of energy transfered by tides into the modes must be equal to the amount of energy dissipated by viscosity: $E_c = \Delta E_{\nu}$. From this condition and equation (29) and (33) we easily obtain an explicit expression for the inverse dissipation time

$$\sigma_{\nu} = \frac{\sigma_k^2 a_{k,k}}{N_k}. \tag{34}$$

Similar arguments can be used for calculations of the amount of the angular momentum transferred to the modes after the fly by. However, the expression for the angular momentum transfer directly follows from the general relation between canonical energy and angular momentum corresponding to a particular mode with given values of k and m (eg. Friedman and Schutz 1977)

$$L_c = mE_c/\sigma_k. \tag{35}$$

Accordingly, we have from equation (29)

$$L_c = 16\pi^3 \sum_{2,k} \sigma_k \frac{S_k S_k^*}{N_k}. \tag{36}$$

The expression for the energy of the modes in the inertial frame, E_I, follows directly from equations (29) and (36)

$$E_I = E_c + \Omega L_c = 8\pi^3 \left\{ \sum_{2,k} \left(\sigma_k(\sigma_k + 2\Omega) \frac{S_k S_k^*}{N_k} \right) + \sum_{0,k} \sigma_k^2 \frac{S_k S_k^*}{N_k} \right\}. \tag{37}$$

Note that the modal energy in the inertial frame can be negative.

3 RESPONSE OF LOW FREQUENCY MODES TO THE TIDAL FORCING

The formalism developed in the previous Section can be applied for any pulsational mode of a rotating planet. It follows from equations (23), (29) and (36) that in order to find the transfer of energy and angular momentum from the orbit to the modes we should be able to find solutions (eigen functions and eigen frequencies) of equation (15) describing free oscillations of the planet. This can be done numerically. However, in general, it is rather difficult to use numerical methods directly in solving equation (15) without any further simplifications. It turns out that these simplifications can be naturally introduced into the problem on hand. Assuming that the periastron distance r_p is sufficiently large, there is a small parameter in the problem, namely the ratio of the typical frequency associated with the periastron passage, $\Omega_p \sim \sqrt{\frac{GM}{r_p^3}}$ to the typical frequency associated with the planet, $\Omega_* = \sqrt{\frac{GM_*}{R_*^3}}$: $\Omega_p \ll \Omega_*$ [2]. We would expect that the angular momentum transfer between the orbit and the modes leads to a so called state of pseudo synchronisation where $\Omega \sim \Omega_p$, and therefore the angular velocity of the planet can be, typically, much smaller than the characteristic frequency Ω_*. In such a situation all modes of pulsation present in a convective planet can be divided in two distinct groups: high frequency modes with eigen frequencies of the order of or larger than Ω_*, and low frequency modes with eigen frequencies of the order of $\Omega \sim \Omega_p$. For the high frequency modes, the effects of rotation on the structure of eigen functions and eigen frequencies can be taken into account as a perturbation (see eg. IP) and references therein). Calculation of the eigen spectrum of the low frequency modes is much more difficult (Papaloizou & Pringle 1981, hereafter PP). However, a convenient approximation can also be made in this case which allows one to reduce the general equation (15) to a much simpler equation for the low frequency modes only (PP, PI).

---

[2] Let us recall that R_* and M_* are the radius and the mass of the planet, respectively, and M is the mass of the object exerting tides on the planet.

3.1 Eigen problem for low frequency modes

In order to reduce equation (15) to an expression appropriate for low frequency modes it is convenient to use the potential $\tilde{W}_m$ (see equation (4) for definition) as a dynamical variable instead of the displacement vector $\tilde{\boldsymbol{\xi}}_m$. We express the components of $\tilde{\boldsymbol{\xi}}_m$ in terms of $\tilde{W}_m$ using the Fourier transformed variant of equation (3) having set $\boldsymbol{f}_\nu = 0$ there. For a normal mode labelled by k, the components of the displacement vector are related to the potential through:

$$\xi_{\varpi,k} = \frac{1}{\sigma_k d_k}\left(-\sigma_k \frac{\partial W_k}{\partial \varpi} + \frac{2m\Omega}{\varpi} W_k\right), \tag{38}$$

$$\xi_{\phi,k} = \frac{i}{\sigma_k d_k}\left(-\frac{\sigma_k m}{\varpi} W_k + 2\Omega \frac{\partial W_k}{\partial \varpi}\right), \tag{39}$$

$$\xi_{z,k} = \frac{1}{\sigma_k^2}\frac{\partial W_k}{\partial z}, \tag{40}$$

where $d_k = 4\Omega^2 - \sigma_k^2$. To simplify notation we shall not use tildes and subscripts denoting m for quantities associated with eigen modes.

Now we substitute equations (38), (39) and (40) into right hand side of the continuity equation (6). The density perturbation on the right hand side is expressed in terms of W_k and perturbed gravitational potential Ψ_k^{int} with help of equation (4) where we set $\Psi^{ext} = 0$. We then obtain

$$\sigma_k^2 \boldsymbol{A} W_k - \sigma_k \boldsymbol{B} W_k - \boldsymbol{C} W_k = \sigma_k^2 d_k \frac{\rho}{c_s^2}(\Psi_k^{int} - W_k), \tag{41}$$

and

$$\boldsymbol{A} = -\frac{1}{\varpi}\frac{\partial}{\partial \varpi}\left(\varpi \rho \frac{\partial}{\partial \varpi}\right) - \frac{\partial}{\partial z}\left(\rho \frac{\partial}{\partial z}\right) + \frac{m^2 \rho}{\varpi^2}, \tag{42}$$

$$\boldsymbol{B} = -\frac{2m\Omega}{\varpi}\frac{\partial \rho}{\partial \varpi}, \quad \boldsymbol{C} = -4\Omega^2 \frac{\partial}{\partial z}\left(\rho \frac{\partial}{\partial z}\right). \tag{43}$$

Note that the operator $\boldsymbol{A}$ can be represented in an invariant form

$$\boldsymbol{A} = -\nabla^\alpha(\rho \nabla_\alpha). \tag{44}$$

As follows from equation (44), $\boldsymbol{A}$ is just a modified Laplace operator.

The operators $\boldsymbol{A}$, $\boldsymbol{B}$ and $\boldsymbol{C}$ are analogous to the operators $\boldsymbol{\mathcal{B}}$ and $\boldsymbol{\mathcal{C}}$ introduced above. They are self-adjoint with respect to the inner product (2). Also when W is not a constant $\boldsymbol{A}$ and $\boldsymbol{B}$ are positive definite and $\boldsymbol{C}$ is non negative definite.

Note that an analogous equation used by PI has a factor $\sigma^2(4\Omega^2-\sigma^2)$ instead of $\sigma_k^2 d_k$ on the right hand side. Accordingly, the potential W_k^{PI} used by PI is different from the potential W_k used in this Paper: $W_k^{PI}=(\frac{\sigma}{\sigma_k})^2(\frac{d}{d_k})W_k$.

Equation for the perturbed gravitational potential Ψ_k^{int} is obtained from equations (4) and (7)

$$\Delta\Psi_k^{int}+\frac{4\pi G\rho}{c_s^2}\Psi_k^{int}=\frac{4\pi G\rho}{c_s^2}W_k \tag{45}$$

Equations (41) and (45) form a complete set. They are equivalent to equation (18) and can be used instead of it to find the solutions for the eigen modes.

Assuming that $\sigma_k\sim\Omega$ it is easy to see that the terms on the right hand side of equation (41) are much smaller than the terms on the left hand side. In the leading approximation in the small parameter $(\Omega/\Omega_*)^2$ they can be neglected and we obtain

$$\sigma_k^2\boldsymbol{A}W_k-\sigma\boldsymbol{B}W_k-\boldsymbol{C}W_k=0. \tag{46}$$

Equation (46) can be used for calculation of the low frequency eigen functions and eigen frequencies. Then a formalism exactly equivalent to that given by PI is obtained.

3.1.1 Equation (46) as a self adjoint problem

Equation (46) can be brought into the standard self adjoint form analogous to equation (18) (PI). For that let us consider two dimensional vector $\vec{Y}_k$ with components

$$Y_k^1=\sigma\boldsymbol{A}^{1/2}W_k,\quad Y_k^2=\boldsymbol{C}^{1/2}W_k. \tag{47}$$

Now it follows from (46) that it can be written in the form

$$\sigma_k\vec{Y}_k=\boldsymbol{H}\vec{Y}_k, \tag{48}$$

where

$$\boldsymbol{H}=\begin{pmatrix}\boldsymbol{A}^{-1/2}\boldsymbol{B}\boldsymbol{A}^{-1/2} & \boldsymbol{A}^{-1/2}\boldsymbol{C}^{1/2}\\ \boldsymbol{C}^{1/2}\boldsymbol{A}^{-1/2} & 0\end{pmatrix}. \tag{49}$$

Since the off diagonal terms in the matrix (49) are adjoint of each other and the diagonal terms are self adjoint it is clear that the operator $\boldsymbol{H}$ has the required self adjoint form.

The inner product induced by the operator $\boldsymbol{H}$ is

$$<< \vec{Y}_k|\vec{Y}_l >>= \sigma_k\sigma_l(W_k|\boldsymbol{A}W_l) + (W_k|\boldsymbol{C}W_l). \tag{50}$$

It is obvious that different solutions of equation (48) are orthogonal with respect to this product.

From equations (21), $(38-40)$ and (50) it follows that the norm N_k corresponding to the displacement vector associated with W_k is related to the norm $n_k = \sigma_k^2(W_k|\boldsymbol{A}W_k) + (W_k|\boldsymbol{C}W_k)$ induced by the inner product (50) as

$$N_k = n_k/(\sigma_k^2 d_k). \tag{51}$$

The density perturbation determined by a solution of equation (48) follows from equation (4)

$$\rho^{'} = \frac{\rho}{c_s^2}(W_k - \Psi_k^{int}), \tag{52}$$

where the gravitational potential Ψ_k^{int} is found from equation (45) with W_k as a source.

The coefficients S_k determining the energy and angular momentum transfer (see equations (29) and (36)) follow from equations (23) and (52). We have

$$S_k = \int \varpi d\varpi dz \frac{\rho}{c_s^2}(W_k - \Psi_k)\Psi^{ext}, \tag{53}$$

where we take into account that we can use real expressions for the potentials W_k and Ψ^{ext}.

The expression (53) can be brought in a simpler form. For that, let us formally solve equation (45)

$$\Psi_k^{int} = 4\pi G \Delta_*^{-1}\frac{\rho}{c_s^2}W_k, \tag{54}$$

where Δ_*^{-1} is the inverse of the operator $\Delta_* = \Delta + \frac{4\pi G\rho}{c_s^2}$. It is easy to see that Δ_*^{-1} is self adjoint. We may, therefore, write the last term on the right hand side of (53) as

$$\int \varpi d\varpi dz \frac{\rho}{c_s^2}\Psi_k\Psi^{ext} = 4\pi G\int \varpi d\varpi dz \frac{\rho}{c_s^2}(\Delta_*^{-1}\frac{\rho}{c_s^2}W_k)\Psi^{ext} = -\int \varpi d\varpi dz\frac{\rho}{c_s^2}W_k\Psi^1, \tag{55}$$

where the potential Ψ^1 is determined from equation analogous to equation (45) but with negative of the potential Ψ^{ext} as a source

$$\Delta\Psi^1 + \frac{4\pi G\rho}{c_s^2}\Psi^1 = -\frac{4\pi G\rho}{c_s^2}\Psi^{ext}. \tag{56}$$

The 'polarisation' potential Ψ^1 has a simple physical meaning. If the external potential Ψ^{ext} is assumed to be static, the potential Ψ^1 is induced in the star by the corresponding perturbation of density.

Finally we obtain

$$S_k = \int \varpi d\varpi dz \frac{\rho}{c_s^2} W_k(\Psi^{ext} + \Psi^1). \tag{57}$$

4 EXPLICIT EXPRESSIONS FOR THE ENERGY AND ANGULAR MOMENTUM TRANSFER

In this Section we obtain explicit expressions for the transfer of energy and angular momentum in terms of quantities characterising the perturbing tidal field and quantities characterising the planet. These will be applied directly to the problem of evaluating the tidal response during a fly by or as a consequence of multiple encounters during circularisation from a highly eccentric orbit. Since the expressions for the energy transfer for the fundamental and p modes are well known (see PT, PI, IP and references therein) we consider only the low frequency modes in this section.

4.1 Fourier transform of the tidal potential

As we have mentioned before we consider highly eccentric orbits in this Paper, with eccentricity $e \sim 1$. In this case the energy and angular momentum transfer takes place mainly near the periastron r_p and we make the usual approximation of the orbit as a parabolic one with the same value of r_p for calculation of the perturbing potential $\tilde{\Psi}^{ext}_m$.

The Fourier's transform of the perturbing potential $\tilde{\Psi}^{ext}$ for the parabolic orbit in the quadrupole approximation has been calculated by PT. We have

$$\tilde{\Psi}^{ext}_m = \sqrt{\frac{5}{2\pi^3}\frac{(2-|m|)!}{(2+|m|)!}}\frac{B_{|m|}}{(1+q)} I_{2,-m}(y)\Omega_p r^2 P_2^{|m|}(\cos\theta), \tag{58}$$

where $B_2 = \sqrt{\frac{3\pi}{10}}$, $B_0 = -\frac{1}{2}\sqrt{\frac{\pi}{5}}$. q is the ratio of M_* to the mass of the star exerting the tides, M: $q = M_*/M$. In the application of our formalism to the problem of circularisation of the extra solar planets $q \sim 10^{-3}$ is very small and will be neglected later.

$$\Omega_p = \sqrt{\frac{GM(1+q)}{r_p^3}} \tag{59}$$

is a typical frequency of periastron passage. The functions

$$I_{2,-m}(y) = \int_0^\infty dx(1+x^2)^{-2}\cos[\sqrt{2}y(x+x^3/3) + 2m\arctan(x)] \tag{60}$$

specify the dependence of $\tilde{\Psi}^{ext}_m$ on σ, they are described by PT. y=$\bar{\Omega}(\bar{\sigma}+m)$, where we use dimensionless frequencies

$$\bar{\sigma} = \sigma/\Omega, \quad \bar{\Omega} = \Omega/\Omega_p. \tag{61}$$

$P_l^m(x)$ is the associated Legendre function, and (r, θ) are the spherical coordinates.

When $y \gg 1$ the quantities $I_{2,-m}(y)$ decay exponentially. This is valid for the case of the high frequency fundamental and p modes where $\bar{\sigma}_k \bar{\Omega} \gg 1$ for the eigen frequencies. On the other hand, the low frequency modes considered above have $\bar{\sigma}_k \sim 1$ and do not experience this suppression.

4.2 First passage problem

The expressions for the energy and angular momentum transfer (34) and (36) are strictly valid only under assumption that the planet is unperturbed before the fly by, and we call the problem formulated in such a way as a 'first passage' problem. This assumption may not be correct when the orbit of the planet is elliptical and the viscous time $t_\nu = 1/\sigma_\nu$ is larger than the orbital period P_{orb}. In latter case the energy and angular momentum exchange between the orbit and the modes depends on the state of the pulsational modes before the periastron passage. However, the expressions for the first passage problem provides a basis for a treatment of that more complicated case, and firstly we would like to discuss this problem. The generalisation to the case of a multi-passage problem is discussed in the next Section.

In our discussion below we assume that effects determined by perturbations of the structure of the planet due to rotation are not significant for our purposes. We use, accordingly, spherical models of the planet in order to find the form of the density and the sound speed entering in equations (30), (36). In the same approximation, taking into account that the perturbing potential is proportional to the product of a function of the radius $r = \sqrt{\varpi^2 + z^2}$ and a spherical harmonic, we see that the variables in equation (56) can be separated in spherical polar coordinates. Therefore we can express the sum $\Psi^{ext} + \Psi^1$ entering in equation (57) as

$$\Psi^{ext} + \Psi^1 = F(r)\Psi^{ext}, \qquad (62)$$

where the function $F(r)$ can be obtained from equation (56).

In order to present the expressions (30), (36) and (37) in a simpler form we express the quantities E_c, E_I and L_c in terms of natural units of energy $E_* = GM_*^2/R_*$ and angular momentum $L_* = M_*\sqrt{(GM_*R_*)}$. As above we also adopt dimensionless units for the spatial coordinates, density and the sound speed expressing them in units of R_*, the averaged density $\bar{\rho} = \frac{3M_*}{4\pi R_*^3}$, and $\sqrt{\frac{GM_*}{R_*}}$, respectively.

Instead of the separation distance r_p it is convenient to introduce the parameter (PT)

$$\eta = \Omega_*/\Omega_p = \sqrt{\frac{1}{(1+q)}\frac{M_*}{M}\frac{r_p^3}{R_*^3}}. \tag{63}$$

We then substitute equations (57) and (62) into (29) and (36). We obtain

$$E_m = \frac{C_m}{(1+q)^2}\bar{\Omega}^4 \sum_k \{\bar{\sigma}_k^4(4-\bar{\sigma}_k^2)Q_k^2 I_{2,-m}^2(y_k)\}\frac{E_*}{\eta^6}, \tag{64}$$

$$L_2 = \frac{2C_2}{(1+q)^2}\bar{\Omega}^3 \sum_k \{\bar{\sigma}_k^3(4-\bar{\sigma}_k^2)Q_k^2 I_{2,-m}^2(y_k)\}\frac{L_*}{\eta^5}, \tag{65}$$

where we separate contributions to E_c and L_c corresponding to different values of m such as $E_c = \sum_{m=0,2} E_m$ and take into account that $L_0 = 0$ and therefore $L_c = L_2$. All quantities in equations (64), (65) are assumed to be in the dimensionless form, $C_2 = \frac{3}{16}$, $C_0 = 3/4$ and

$$y_k = \bar{\Omega}(\bar{\sigma}_{(k)} + 2). \tag{66}$$

The overlap integrals Q_k are analogous to the same quantities introduced by PT in their analysis of dynamic tides in a non rotating star. They describe spatial coupling of the perturbing potential and of the eigen modes, and have the form:

$$Q_k = (\frac{\rho}{c_s^2}F(r)r^2P_2^m|W_k)/\sqrt{\bar{n}_k}, \tag{67}$$

where $\bar{n}_k = n_k/\Omega^2$.

The expression (64) and (65) have already been obtained by PI using a different method. They can also be presented in another equivalent form as

$$E_m = \frac{\epsilon_m(\bar{\Omega})}{(1+q)^2\eta^6}E_*, \quad L_2 = \frac{\lambda(\bar{\Omega})}{(1+q)^2\eta^5}L_*, \tag{68}$$

where the dependence of the functions ϵ_m and λ on $\bar{\Omega}$ follows from (64) and (65). Accordingly, the energy transfer in the inertial frame follows from (37), (68) and the use of

$$\epsilon_m = C_m\bar{\Omega}^4 \sum_{(k)} \bar{\sigma}_{(k)}^4(4-\bar{\sigma}_{(k)}^2)Q_{(k)}^2 I_{2,-m}^2(y_k), \tag{69}$$

where all quantities in the brackets belong to a particular value of $m = 0, 2$,

$$\lambda = 2C_2\bar{\Omega}^3 \sum_{(k)} \bar{\sigma}_{(k)}^3(4-\bar{\sigma}_{(k)}^2)Q_{(k)}^2 I_{2,-2}^2(y_k), \tag{70}$$

where all quantities in the brackets are evaluated for $m = 2$ and

$$\epsilon_I = \epsilon_2 + \bar{\Omega}\lambda, \tag{71}$$

as

$$E_I = \frac{(\epsilon_0 + \epsilon_2 + \bar{\Omega}\lambda)}{(1+q)^2\eta^6}E_* \;=\; \frac{(\epsilon_0 + \epsilon_I)}{(1+q)^2\eta^6}E_*. \tag{72}$$

Usually, the moment of inertia of the planet is much smaller than the moment of inertia of the orbit. In this case the planet tends to rotate with 'equilibrium' value of the angular velocity, Ω_{eq} determined by condition that there is no exchange of angular momentum between the planet and the orbit at this rotation rate,

$$\lambda(\Omega_{eq}) = 0. \tag{73}$$

This state of rotation is often referred to as a state of 'pseudo-synchronisation'. For a given model of planet, equation (73) can be solved numerically to find Ω_{eq}. The expression for the energy transfer at the state of 'pseudo-synchronisation', E_{ps}, follows from equation (72)

$$E_{ps} = \frac{\epsilon_*}{\eta^6} E_*, \tag{74}$$

where $\epsilon_* = \Sigma_m \epsilon_m(\Omega_{eq})$ depends only on the structure of a planet. For simplicity we set $1+q=1$ hereafter. The expressions for a comparable mass ratio q can be easily obtained from our equations by an appropriate re-scaling of variables we use.

An estimate of ϵ_* can be obtained from the following semi-analytical arguments. As we will see below only two 'global' modes with $m = 2$ mainly determine the energy transfer when $\Omega \sim \Omega_{eq}$ and we can take into account only these two modes in the summation (73) and (74). One of these modes has a positive eigen frequency with $\bar{\sigma}_1 \approx 0.6$ and the overlap integral $Q_1 \approx 0.16$, and another mode has a negative eigen frequency with $\bar{\sigma}_2 \sim -1.1$. The equilibrium value of the angular velocity is always close to the frequency of periastron passage, with $\bar{\Omega}_{eq} \approx 1.55$. This information is sufficient to estimate ϵ_*. Indeed, we can express the second overlap integral from equation (73) in terms of Q_1, the eigen frequencies and the quantities $I_{2,-2}(y_{1,2})$, where $y_{1,2} = \bar{\Omega}_{eq}(2+\sigma_{1,2})$. We get $Q_2 \sim 0.033$. Taking into account that $I_{2,-2}(y_1) \approx 0.32$ and $I_{2,-2}(y_2) \approx 0.74$, we get $\epsilon_* \sim 4 \cdot 10^{-3}$. This value is in a good agreement with numerical results discussed below, see discussion and equation (98) in Section 6. Note that for $n = 1.5$ polytrope $\epsilon_* \approx 6.5 \cdot 10^{-3}$ (PI).

4.3 Multi-passage problem

In the circularisation problem expressions (29), (36), (37), (64), (65), (68), (72) and (74) are strictly valid only when the energy stored in the modes can be dissipated between two successive periastron passages. In the opposite limit, when the dissipation time $t_\nu \gg P_{orb}$, where P_{orb} is the orbital period, the planet approaches periastron in a perturbed state. The additional linear perturbation induced during a particular periastron passage must be added to the perturbation already present in the star. Since the mode energy is quadratic in the perturbed quantities, it can either decrease or increase after the periastron passage, depending on phase of the perturbations (Kochanek, 1992, Mardling 1995a, 1995b). This issue has been studied analytically by IP. It was found that when a change of the orbital period between two successive periastron passages is sufficiently large, the energy transfer proceeds in a stochastic way. In this case the phase of perturbation in the planet approaching periastron is not correlated with the phase of the perturbation induced by tides near periastron, and the energy transfer during the periastron passage is essentially a random quantity, with dispersion of the order of the expressions for the energy transfer calculated above. In this situation, a build-up of mode energy due to stochastic instability is possible. A semi-analytical condition for this instability to happen has been obtained in IP. Here we generalise their formalism to take account of the specific features associated with inertial waves.

Let us assume that dissipation is negligible and treat the tidal influence as a sequence of impulses separated by periods of time equal to the orbital period. In this case, any time between two impulses the planet undergoes free oscillation, and the Lagrangian displacement vector can be represented by an expression analogous to (27)

$$\boldsymbol{\xi} = 2\pi i \sum_{m,k} \left(\frac{\sigma_k S_k}{N_k} A_k e^{i\psi_k} e^{-i\sigma_k t} e^{im\phi} \boldsymbol{\xi}_k + c.c.\right), \tag{75}$$

where the dimensionless real coefficients $A_k \geqslant 1$ characterise the amplitudes of perturbations corresponding to different modes and ψ_k are the corresponding phases. Note that the origin of time is chosen to coincide with the moment of periastron passage. The expressions for the canonical energy and angular momentum follow from (28), (35) and (75)

$$E_c = 8\pi^3 \sum_{m,k} A_k^2 \frac{\sigma_k^2 S_k S_k^*}{N_k}, \quad L_c = 16\pi^3 \sum_{m=2,k} A_k^2 \sigma_k \frac{S_k S_k^*}{N_k}. \tag{76}$$

When $A_k = 1$ these expressions obviously coincide with the expressions (29) and (36) for the single passage problem. For inertial waves equations (76) can be brought to the form analogous to equations $(68-70)$

$$E_m = \left(\sum_k \epsilon_{m,k} A_k^2\right) \frac{E_*}{(1+q)^2 \eta^6}, \quad L_2 = \left(\sum_k \lambda_k A_k^2\right) \frac{L_*}{(1+q)^2 \eta^5}, \tag{77}$$

where we now show separately the contributions of terms with different m to the canonical energy. $\epsilon_{m,k}$ and λ_k are the terms in the summation series for ϵ_m and λ, corresponding to a particular value of k, see equations (68), (69) and (70). As we discus below in the tidal problem we can neglect the contribution of $m = 0$ terms. In this case, the mode energy in the inertial frame can be represented as

$$E_I = \left(\sum_{m=2,k} \frac{(\epsilon_{2,k} + \bar{\Omega}\lambda)}{\epsilon_*} A_k^2 \right) E_{ps}, \tag{78}$$

where E_{ps} is given by (74)

After the periastron passage, the expression (27) must be added to (75), and the resulting expression can brought again to the form (75) but with new values of the amplitudes and phases, A_k^n and ψ_k^n. Thus, the action of tidal forcing defines an iterative map $(A_k^{n-1}, \psi_k^{n-1}) \rightarrow (A_k^n, \psi_k^n)$. It is convenient to introduce new variables $(x_k^{n-1}, x_k^n) = (A_k^{n-1}\cos\psi_k^{n-1}, A_k^n \cos\psi_k^n)$ and $(y_k^{n-1}, y_k^n) = (A_k^{n-1}\sin\psi_k^{n-1}, A_k^n\sin\psi_k^n)$. In terms of these variables this map has especially simple form (IP)

$$\begin{pmatrix} x_k^n \\ y_k^n \end{pmatrix} = \boldsymbol{R}(-\phi_k) \begin{pmatrix} x_k^{n-1} + 1 \\ y_k^{n-1} \end{pmatrix}, \tag{79}$$

where $\phi_k = \sigma_k P_{orb}$, and $\boldsymbol{R}(\phi)$ is a two dimensional rotational matrix. Note that in equation (79) we take into account the change of origin of time after the periastron passage: $t \rightarrow t + P_{orb}$.

When P_{orb} is a constant, it is easy to see from equation (79) that the amplitudes A_k^n do not grow with the number of iterations. However, the orbital period depends on the orbital energy, E_{orb}, as

$$P_{orb} = \frac{\pi G M^{5/2} q^{3/2}}{\sqrt{2|E_{orb}|}|E_{orb}|(1+q)^{1/2}}, \tag{80}$$

and the orbital energy is proportional to the mode energy E_I due to the law of energy conservation. Since $E_I = \left(\sum_{k,2} \frac{(\epsilon_{2,k}+\bar{\Omega}\lambda)}{\epsilon_*}(A_k^{n-1})^2\right) E_{ps}$ is proportional to the squares of the modes amplitudes, A_k^{n-1}, the map is non-linear.

In order to simplify the problem, let us consider a situation when the mode energy is much smaller than the orbital energy such that the orbital energy and angular momentum remain in the neighbourhood of some particular fixed values. In this case we can set $P_{orb} = P_{orb}(0) + \Delta P_{orb}$, where $P_{orb}(0)$ is a constant, and

$$\Delta P_{orb} = -\frac{3}{2}\frac{P_{orb}}{|E_{orb}|}\frac{E_I}{M_*} = -6\pi\sqrt{\frac{a^5}{(GM)^3}}\frac{E_I}{M_*}, \tag{81}$$

where E_{orb} and a are the orbital energy and semi-major axis corresponding to the period $P_{orb}(0)$. Now the angles ϕ_k can be expressed in terms of E_I as

$$\phi_k = \phi_k(0) - \bar{\sigma}_k \alpha \tilde{E}_I, \tag{82}$$

where $\tilde{E}_I = E_I/E_{ps}$, $\phi_k(0) = \sigma_k P_{orb}(0)$ and

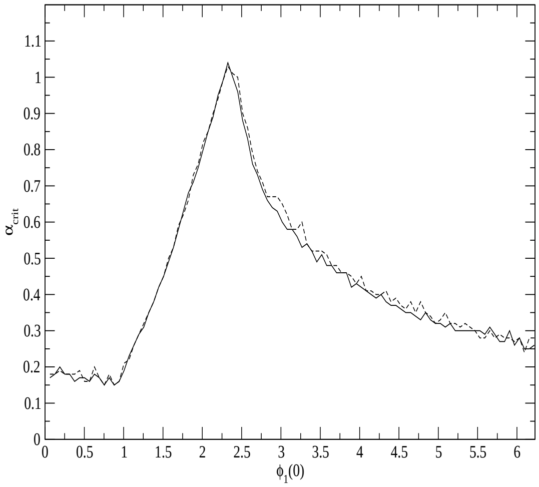

Figure 1. The dependence of α_{crit} on $\phi_1(0)$. The solid and dashed lines correspond to the maximal number of iterations $N_{max} = 10^5$ and $N_{max} = 10^4$, respectively.

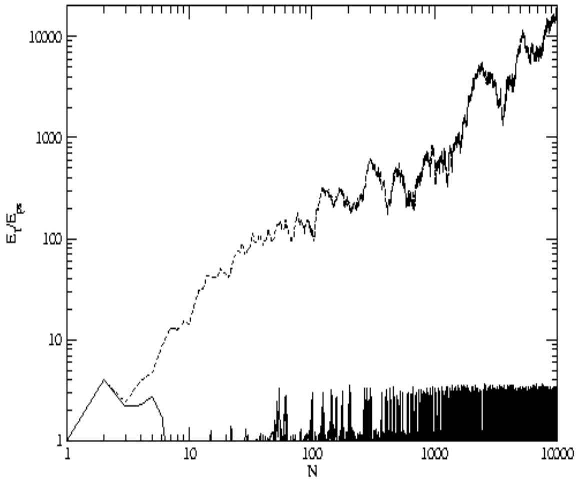

Figure 2. $\tilde{E}_I$ as a function of the number of iterations N. The case $\phi_1(0) = 2.32$ corresponding to the maximal value of $\alpha_{crit} = 1.04$ is shown. The solid curve corresponds to $\alpha = 0.9$ and the dashed curve corresponds to $\alpha = 1.1$.

$$\alpha = 6\pi\epsilon_* \bar{\Omega} \frac{M_*}{M} \frac{1}{\eta^6} \left(\frac{a^{5/2}}{r_p^{3/2} R_*} \right), \tag{83}$$

where we use equations (61), (63), (74) and (81). Equation (83) is analogous to equation (84) of IP.

Equations (78), (79) and (83) fully determine the map for given values of $\phi_k(0)$ *mod* 2π and α. When α are sufficiently large, stochastic instability sets in. Since the angles $\phi_k(0)$ are determined by initial conditions, the results should be averaged over these angles.

This map has been investigated numerically by IP for the case of only one high frequency mode. It has been found that the instability sets in when the average value of α is larger than $\alpha_{crit} \approx 0.67$. In our case the situation is slightly more complicated since there are at least two modes which play a role in the energy transfer. Also, we should specify the evolution of the angular velocity. In order to investigate this question we consider numerically the simplest possible case of constant equilibrium rotation of a planet, when $\bar{\Omega} = \bar{\Omega}_{eq}$. For definiteness, we use parameters described in the end of the previous section, namely $\bar{\Omega}_{eq} = 1.55$ and consider only $m = 2$ modes with $\bar{\sigma}_1 = 0.6$ and $\bar{\sigma}_2 = -1.1$. In this case we have $\epsilon_2 \approx 0.35\epsilon_*$ in the first case and $\epsilon_2 \approx 0.65\epsilon_*$ in the second. We iterate numerically the map for a large number N of iterations for a given value of $\phi_1(0)$ with $\phi_2(0) = \frac{\bar{\sigma}_2}{\bar{\sigma}_1}\phi_1(0)$, and for a given value of α. The stochastic instability is assumed to set in when the energy $\tilde{E}_I$ exceeds the maximal number of iterations, N_{max} during the iterations. This happens when α exceeds some critical value $\alpha_{crit}(\phi_1(0))$. The results of our computations are shown in Figure 1. One can see from this Figure that there is a strong dependence of α_{crit} on $\phi_1(0)$. Nevertheless we use the averaged value of α_{crit}, $\bar{\alpha}_{crit} = \frac{1}{2\pi}\int_0^{2\pi}\alpha_{crit} \approx 0.43$ since our results are rather insensitive to the exact values of α_{crit}. It is interesting to note that the transition from a quasi-periodic behaviour of $\tilde{E}_I$ to stochastic behaviour is very sharp. In Figure 2 we show the evolution of $\tilde{E}_I$ for $\phi_1(0) = 2.32$ and two values of α: $\alpha = 0.9 < \alpha_{crit} = 1.04$ and $\alpha = 1.1 > \alpha_{crit} = 1.04$. One can see from this Figure that a small change of α is sufficient for stochastic instability to set in.

From the condition $\alpha > \alpha_{crit}$ we find that the stochastic instability sets in only when the semi-major axis is sufficiently large,

$$a > a_{st} = (\frac{\alpha_{crit}}{6\pi\bar{\Omega}_{ps}\epsilon_*})^{2/5}\left(\frac{M}{M_*}\right)^{3/5}\eta^{14/5}R_*. \tag{84}$$

Using the values of all quantities in (84) typical for the problem of circularisation of extra solar planets, we have

$$a_{st} \approx 30\left(\frac{M_J}{M_*}\right)^{3/5}\left(\frac{M}{M_\odot}\right)^{3/5}(\frac{R_*}{R_J})\eta_{10}^{14/5}au, \tag{85}$$

where $\eta_{10} = \eta/10$, $M_J \approx 2\cdot 10^{30}g$ and $M_\odot \approx 2\cdot 10^{33}g$ are the masses of Jupiter and of the Sun, respectively, and $R_J \approx 7\cdot 10^9 cm$ is the radius of Jupiter. Remarkably, the typical value of $a_{st} \sim 30au$ is close to what has been obtained in the analysis of the stochastic instability associated with the fundamental modes (IP). This value is of the order of a typical 'initial' semi-major axis from which we would expect the process of circularisation to begin for $\eta = 10$. This corresponds to a final circularised period of 3.3 d for a Jupiter mass planet around a solar type star. However if the final period is reduced to $\sim 1, 2$ d, corresponding to the shortest period exoplanets, the initial semi-major axis is reduced to between 1 and $2au$. If the initial semi-major axis is smaller, the stochastic growth of the mode energy is not possible. However, in this case, we would expect a stronger dissipation of the mode energy due non-linear mode-mode interactions (e.g. Kumar & Goodman 1996). This possibility needs a further investigation.

5 PLANET MODELS AND THEIR NORMAL MODE SPECTRA

In this Section we construct realistic models of planets at different evolutionary stages for which we obtain the oscillation spectra numerically. We discuss our numerical method, use it to solve equation (48), and discuss the results which are used in subsequent sections to evaluate the tidal responses of different planet models undergoing a fly by or circularisation from a highly eccentric orbit.

We find it convenient to adopt a system of dimensionless units for the spatial coordinates, density and the sound speed expressing them in units of R_*, the averaged density $\bar{\rho} = \frac{3M_*}{4\pi R_*^3}$, and $\sqrt{\frac{GM_*}{R_*}}$, respectively. We also use dimensionless frequencies

$$\bar{\sigma} = \sigma/\Omega, \quad \bar{\Omega} = \Omega/\Omega_p. \tag{86}$$

5.1 The planet models

We assume that the planets are spherically symmetric and adopt the equation of state of Saumon, Chabrier & Van Horn (1995). Although it is likely that giant planets form through a nucleated core instability (eg. Bodenheimer & Pollack 1986), for this first set of calculations, for reasons of simplicity we shall assume that solid cores are absent. In this context we note that the mass of any solid core in Jupiter is highly uncertain, being sensitive among other things to the equation of state adopted, with recent estimates showing it to be consistent with zero (see Saumon & Guillot 2004). To make this consistent with a nucleated core instability scenario for formation, these authors suggest that a core could be eroded and remixed during subsequent gas accretion of light elements. But it should be noted that the presence of a large solid core could significantly affect the mode spectrum of the planet through the existence of wave attractors (eg. Ogilvie & Lin 2004) that could produce effects on a long time scale. However, the presence of a small core is unlikely to affect phenomena of short duration such as the energy transfer that occurs during a close passage or fly by.

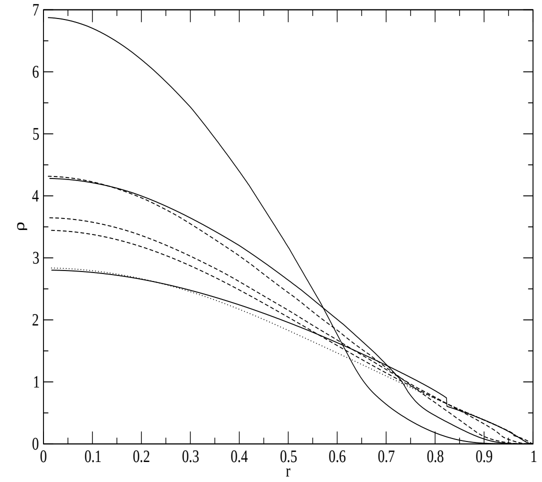

Figure 3. The density ρ scaled in terms of the mean density as a function of the dimensionless radius r. The three solid curves are for models with $M_* = 1M_J$ and radii $R_* = 1R_J$, $1.4R_J$ and $2R_J$ respectively. The three dashed curved are for models with $M_* = 5M_J$ and radii $R_* = 1.03R_J$, $1.4R_J$ and $2R_J$ respectively. The dotted curve corresponds to the model with $M_* = 1M_J$ and radius $R_* = 1R_J$. and 'smoothed' density profile. Curves of the same type starting from larger values at $r = 0$ correspond to planet models with larger radii. Note that because of the use of different scalings to dimensionless variables the numerical values differ from those of IP by a factor $\frac{4\pi}{3}$.

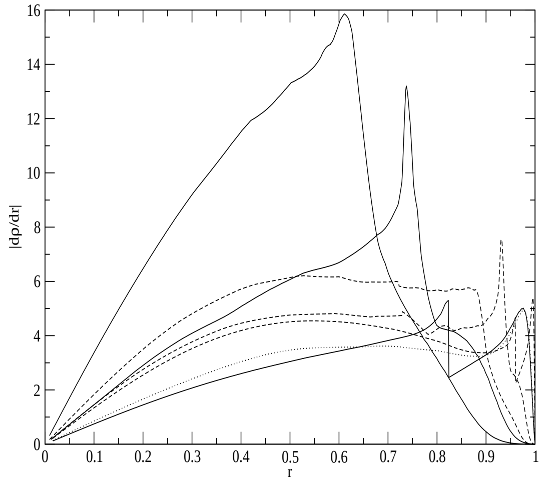

Figure 4. As in Fig. 3 but the absolute value of the density gradient $|\frac{d\rho}{dr}|$ is shown. Curves of the same type starting from larger values at $r = 0$ correspond to planet models with larger radii.

We calculate numerically the form of ρ and c_s as functions of the radius r. With these functions known, equation (48) can be solved and the overlap integrals (67) calculated. As in IP we consider only two planet masses $M_* = 1M_J$ and $5M_J$.

For a given mass we calculate planet models for six values of the radius. These are $R_* = 1R_J$ ($R_* = 1.03R_J$) when $M_* = M_J$ ($M_* = 5M_J$), and $R_* = 1.2R_J$, $1.4R_J$, $1.6R_J$, $1.8R_J$, $2R_J$ for both masses. The different values of radius for a given mass correspond to different points on an evolutionary track. On such a track, the radius decreases with time

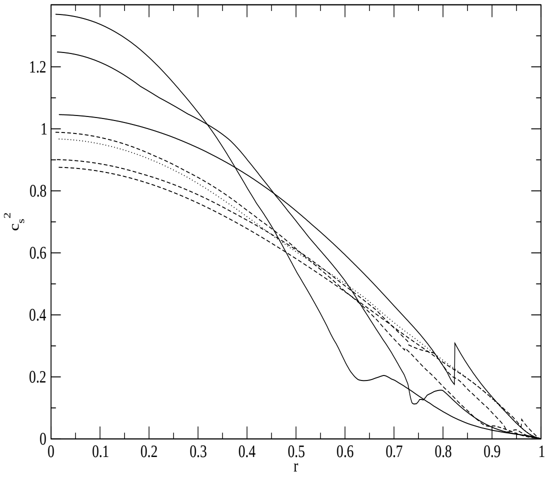

Figure 5. As for Fig. 3 and Fig. 4 but the square of sound speed c_s^2 is shown. Curves of the same type starting from larger values at $r = 0$ correspond to planet models with larger radii.

due to gravitational contraction. To determine the age corresponding to a given radius, we use the relationship between the radius and luminosity, and hence the age of the planet calculated by Burrows et al (1997) (see Fig. 8 of IP). Since a young hot planet of age $\sim 10^6 yr$ has a radius of around $\sim 2R_J$, the range of radii we consider corresponds to planet ages between $\sim 10^6 yr$ and $\sim 5 \cdot 10^9 - 10^{10} yr$.

We illustrate the dependences of the density, the magnitude of the density gradient $|\frac{d\rho}{dr}|$ and square of the sound speed for several planet models in Figures 3-5. As one can see from Figure 3 for a particular planet, the ratio of central density to mean density increases with radius. This effect is less prominent for the models with $M_* = 5M_J$.

Note a sharp drop of density at $r \approx 0.82$ when $M_* = 1M_J$, and $R_* = 1R_J$. This is due to the phase transition of hydrogen from the metallic to molecular phase which is assumed to be of the first kind. This phase transition also takes place when $M_* = 5M_J$ and $R_* = 1.03R_J$, but it is shifted to a larger $r \approx 0.96$ and is not well resolved in this Figure. In general, according to Saumon, Chabrier & van Horn (1995), the phase transition is of the first kind when $R_* < 1.27R_J$ ($R_* < 1.255R_J$) for $M_* = 1M_J$ ($M_* = 5M_J$). For larger radii the adiabats describing the interiors of the planets go above the critical point of Saumon, Chabrier & van Horn (1995) equation of state on (P, T) phase plane. As we see below the effect of the phase transition on the structure of the eigen spectrum is more prominent for $M_* = 1M_J$.

To illustrate this it is of interest to compare this model with a similar model without the phase transition and we make such a model with 'smoothed out' transition between the metallic and molecular phases (dotted curves in Figures 3-5), for $M_* = 1M_J$ and $R_* = 1R_J$.

This model has been calculated using a prescription provided by Saumon, Chabrier & van Horn 1995.

The structure of the density profiles is better seen in Figure 4 where the magnitudes of the density gradients are plotted. For the models with the phase transition there is a discontinuity at the radius of the phase transition. For the models without the phase transition the modulus of the gradients increase with radius at small r, and they sharply decrease at large r. The transition point between these two limiting cases corresponds to a 'melting' point where the number density of the hydrogen molecules sharply decreases toward smaller values of r. This transition point shifts toward smaller r with increase of the planet radius. As seen from Figure 5 the sound speed is changes non monotonically near the transition point.

In general, the models corresponding to the larger mass are more similar to each other. In this case the radius of transition is shifted toward larger r where the planets have rather low density. The low density outer regions of the planet should not influence eigenfrequencies and eigenfunctions corresponding to global modes should they exist. Therefore, it is reasonable to suppose the presence of the phase transitions and the 'melting' zones in the planet models with $M_* = 5M_J$ is less significant for our problem than for the case of $M_* = 1M_J$. As we see below this assumption is supported by our numerical results.

5.2 Numerical method

For our numerical work we use a method similar to that proposed by PP. This involves reducing the operator equations to discrete form by use of a set of basis functions.

5.2.1 Matrix representation of equations (46) and (48)

For our numerical work it is convenient to work with a matrix representation of equation (46). This is accomplished by use of a basis of 'trial' functions v^j, $j = 1, ..\infty$ which is assumed to be complete. We introduce a Fourier decomposition of an eigenfunction $W_{(k)}$ in terms of the trial functions as

$$W_{(k)} = \sum_j \alpha_j^{(k)} v^j, \tag{87}$$

where the indices enumerating the eigen functions are enclosed in brackets from now on. Then we substitute equation (87) into equation (46) and taking the scalar product (2) of the resulting expression with v^i we get

$$(\sigma_{(k)}^2 A_i^j - \sigma_{(k)} B_i^j - C_i^j)\alpha_j^{(k)} = 0, \tag{88}$$

where

$$A_i^j = (v^i|\boldsymbol{A}v^j), \quad B_i^j = (v^i|\boldsymbol{B}v^j), \quad C_i^j = (v^i|\boldsymbol{C}v^j), \tag{89}$$

and the standard summation rule over the repeating indices is implied [3]. We can introduce square roots and inverses of the above matrices in a similar manner to that adopted for the corresponding operators. Let us consider infinite dimensional vectors analogous to the vectors $\vec{Y}_{(k)}$ (see (47)), with components $Y_M^{(k)}$ where the index M stands for the pair $((1,i)$ and $(2,i))$. We have

$$Y_{1,i}^{(k)} = \sigma_{(k)}(A^{1/2})_i^j \alpha_j^{(k)}, \quad Y_{2,i}^{(k)} = (C^{1/2})_i^j \alpha_j^{(k)}. \tag{90}$$

The eigen value problem (88) can be formulated for the vectors (90) in a way equivalent to (48),

$$\sigma_{(k)} Y_N^{(k)} = H_N^M Y_M^{(k)}, \tag{91}$$

where the matrix H_N^M has a structure equivalent to the operator $\boldsymbol{H}$ (equation (49)) with the operators being substituted by the corresponding matrices.

It is natural to use the solutions of the eigenvalue problem

$$\boldsymbol{A}v^j = \lambda\rho v^j \tag{92}$$

as the functions v^j. These functions are orthogonal with respect to the inner product (2). As follows from equation (44), for the spherical planet models the variables in equation (92) are separable in spherical polar coordinates (r,θ), $v^j = v_{n,l}(r)P_l^m(\cos\theta)$, where $n = 1, 2, ...$ $n-1$ is the order of the radial eigenfunction and the index j stands for the pair of positive integers (n,l). For the radial part we have

$$-\frac{1}{r^2}\frac{d}{dr}\left(r^2\rho(r)\frac{d}{dr}v_{n,l}\right) + \frac{L^2}{r^2}\rho(r)v_{n,l} = \lambda_{n,l}\rho(r)v_{n,l}, \tag{93}$$

where $L = \sqrt{l(l+1)}$. It follows from (93) that the eigen values of $\boldsymbol{A}$ are bound from below: $\lambda_{n,l} \geqslant L^2$ when $l \neq 0$.

5.2.2 Numerical approach

In our numerical work we truncate the series (87) at some sufficiently large value $j = j_{max}$. The trial functions must be arranged in such a way that when j is sufficiently large the corresponding trial functions oscillate with periods of spatial oscillation that decrease with increasing j. In this case, one can argue that errors will be small because of a negligible contribution of the oscillatory terms with high j to the various integrals occurring in the formulation of our problem as discussed above. Of course, this idea must be tested, and we discuss such tests later.

---

[3] We stress that we do not sum over the indices enclosed in the brackets that label an eigenfunction.

Since for our problem $m = 0, 2$ is even and the angular parts of the trial functions are such that $P_l^m(x) = (-1)^l P_l^m(-x)$, the modes odd with respect to reflection in $x \rightarrow -x$ do not couple with the tidal field and we can choose $l \geqslant m$ to be even. Thus $l = 2l_1$ with l_1 being a positive integer such that $l_1 \geqslant m/2$.

It is convenient to consider an equal number of the radial functions $n(max)$ and angular functions $l_1(max)$. Thus we write $n(max) = l_1(max) = N_{max}$. In our numerical work, we use different values of N_{max} in order to study the dependence on the number of trial functions, with the largest $N_{max} = 15$. Accordingly, we have $j_{max} = N_{max}^2 \leqslant 225$.

After truncation of the basis set used in (87) we have ordinary finite dimensional matrices A_i^j, B_i^j and C_i^j. We calculate the eigenvalues eigenvectors of these matrices. The eigenvalues are used to calculate the inverses and square roots of the matrices entering in the matrix H_N^M. We find the components of H_N^M and solve the eigenvalue problem (91). The eigenvectors $Y_N^{(k)}$ are used to find the coefficients $\alpha_j^{(k)}$, and we use these coefficients to find the eigenfunctions $W_{(k)}$ with help of equation (87).

One can view the eigenvalues and eigenfunctions as belonging to the oscillation spectrum of the planet. For the case of a model without a solid core this is ultimately likely to be discrete but everywhere dense (see eg. PP). One should also consider the possibility of the existence of a continuous spectrum in some cases. Then the numerically obtained eigenfunctions may not show convergence to regular functions. But note that, independently of this issue, we expect our numerical method to be convergent when the eigenfunctions we obtain are used to provide a basis for representing smooth functions varying on a global scale. The issue of the possibility of ultimately irregular eigenfunctions belonging to a continuous spectrum does not affect this or preclude the convergence of the process of calculating the angular momentum and energy exchanges associated with a fly by. On account of the forcing by a global potential and short time duration of a fly by, a basis representation capable of representing global scales would be expected to be adequate on physical grounds. Indeed for our models it turns out that only a few global eigenfunctions are important for determining the energy exchanged and these can be represented with a basis set that needs only to be capable of representing global functions. This makes the issue qualitatively different to the one that occurs in the context of tidal forcing occurring in a circular orbit with fixed frequency for infinite time periods (eg.Ogilvie & Lin 2004).

It is obvious that the dimension of the matrix H^M_N is $2j_{max}$. Thus, we have $2j_{max}$ eigen values $\sigma_{(k)}$ and eigen vectors [4]. The number of terms in the series occurring in (64), (65) and (77) determining the tidal response, is proportional to j_{max}. It is important to check whether the process adopted and the corresponding series converges and we discuss this issue below. As we have stressed above, the convergence of the series means that the tidal response is mainly determined by a few 'global' modes with a large scale distribution of $W_{(k)}$ over the planet.

5.2.3 Degenerate modes with $\sigma_{(k)} = 0$ and the case with $m = 0$

The results of our numerical calculations reported below allow us to suggest that the numerical method described above is stable and robust for the modes with sufficiently large values of $|\sigma_{(k)}|$. However, there is a problem with this approach related to the case of small values of $|\sigma_{(k)}| \approx 0$. This problem is associated with the existence of a non-trivial null space of the operator $\boldsymbol{C}$. It is easy to see that all modes satisfying

$$\boldsymbol{C} W_{(k)} = 0 \qquad (94)$$

are degenerate solutions of (46) (and (48)) with $\sigma_{(k)} = 0$. In fact any $W_{(k)}$ that is independent of z will do. The corresponding norm $n_{(k)} = 0$. Physically, for $m = 0$, these modes correspond to introducing an infinitesimal amount of differential rotation and thus slightly shifting the static equilibrium. As follows from equation (67) the overlap integrals are formally infinite for these modes. However, in the exact theory this does not lead to any difficulty since the contribution of a particular mode to the energy exchange is proportional to $\sigma^4_{(k)}$ (see e.g. equation (64). This means that the degenerate set of modes is in fact not excited.

However, due to numerical inaccuracy of our method the modes formally belonging to the null space of $\boldsymbol{C}$ acquire small non zero $\sigma_{(k)}$. The corresponding overlap integrals are very large and they can lead, in principal, to a very large unphysical energy transfer. This problem is not significant for the case of $m = 2$. In this case, the quantities $I_{2,-2}(y)$ entering in (64) are very small for an interesting range of y. They suppress effectively the contribution of the spurious modes to the energy and angular momentum exchange. On the other hand, in the

---

[4] Note that some of $\sigma_{(k)}$ are degenerate.

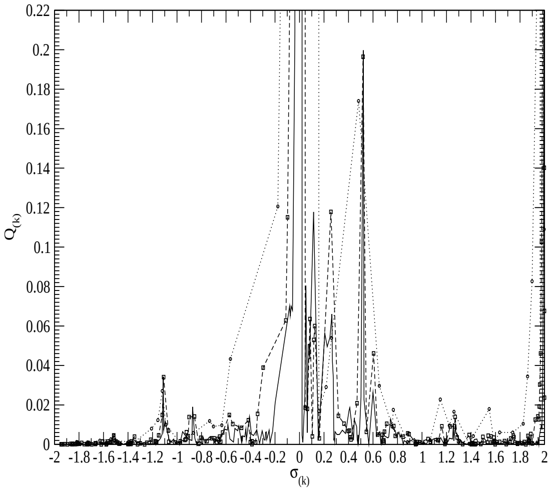

Figure 6. The overlap integrals $Q_{(k)}$ as functions of the eigen frequency $\bar{\sigma}_{(k)}$. The dotted and dashed curves correspond to $j_{max} = 25$ and $j_{max} = 100$ respectively. Circles and squares show the positions of particular $Q_{(k)}$. The solid curve corresponds to the case with $j_{max} = 225$.

case of $m = 0$ the corresponding quantities $I_{2,0}(y)$ do not suppress this contribution, and the spurious modes do lead to a very large unphysical energy transfer. Therefore, in principle, the numerical method must be able to overcome this difficulty, by e.g. incorporating the solutions to (94) in the set of the trial functions.

This can be done by considering polynomials consisting of products of different power of ϖ and z as a new set of trial functions (PP) instead of solutions to (92). However, this set is difficult to use when considering a large values of j_{max}. Therefore, in our numerical work we simply identified the spurious modes corresponding to $m = 0$ by comparing the spectra calculated using these two different sets of trial functions and removed them from the summation in the expression for the transfer of energy (there is no angular momentum exchange in this case). The resulting contribution to the energy exchange appears to be very small compared with what is obtained for the case of $m = 2$, and we will not discuss further the case $m = 0$ below.

5.3 The spectrum of a planet with $M_* = 1M_J$ and $R = 1R_J$

In this Section we discuss in detail the case of a planet with $M_* = 1M_J$ and $R_* = 1R_J$. This case has the most complicated spectrum of all models we consider. In our opinion, this is mainly because of the presence of the phase transition at a sufficiently small radius $r \approx 0.82$. The analysis of the eigenfrequencies and the eigenmodes developed for this case can be easily applied to planets with larger radii and masses which have a simpler structure.

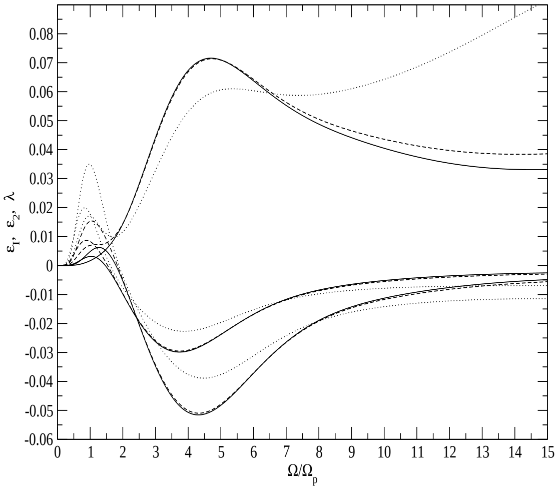

Figure 7. The quantities ϵ_I, ϵ_2 and λ as functions of the dimensionless rotation rate $\bar{\Omega}$. The dotted, dashed and solid curves correspond to $j_{max} = 25$, 100 and 225, respectively. The curves which always pass through positive values represent ϵ_2. The curve of a given type that takes on the least value corresponds to ϵ_I, the remaining curve corresponding to λ.

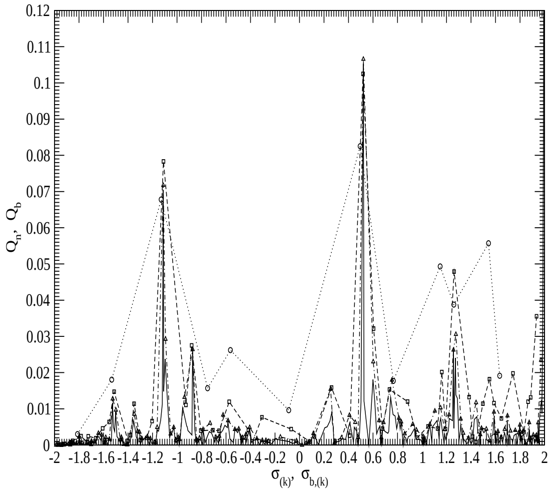

Figure 8. The binned overlap integrals $Q_{b,(k)}$ are plotted for $j_{max} = 25$ using the dotted curve with circles; for $j_{max} = 100$ using the dashed curve with squares; and for $j_{max} = 225$ using the dot-dashed curve with triangles. The solid curve shows the original overlap integrals $Q_{n,(k)}$ calculated for the case of $j_{max} = 225$. Note that the dot-dashed and the solid curves almost coincide.

In Figure 6 we show the overlap integrals $Q_{(k)}$ (see equation (67) for the definition) calculated for this case as a function of the eigenfrequency $\bar{\sigma}_{(k)}$. It can be shown analytically (PP) that $|\bar{\sigma}_{(k)}| < 2$. The curves of different types correspond to different numbers of the trial functions, $j_{max} = 25$, 100 and 225. We show positions of particular $Q_{(k)}$ representing results of calculations with $j_{max} = 25$ and $j_{max} = 100$ as circles and squares, respectively. As we have mentioned above the sharp rise near $\bar{\sigma}_{(k)} \sim 0$ is due to numerical inaccuracy. There is a similar unphysical rise near $\bar{\sigma}_{(k)} \sim 2$. It is clearly seen from Figure 6 that the width

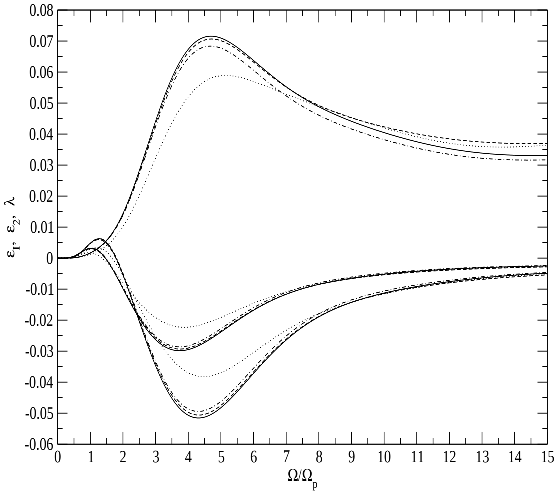

Figure 9. Same as Fig. 7 but now the dotted, dashed and dot-dashed curves are calculated using the binned overlap integrals for $j_{max} = 25$, $j_{max} = 100$ and $j_{max} = 225$, respectively. The solid curve is calculated using the original overlap integrals for the case of $j_{max} = 225$.

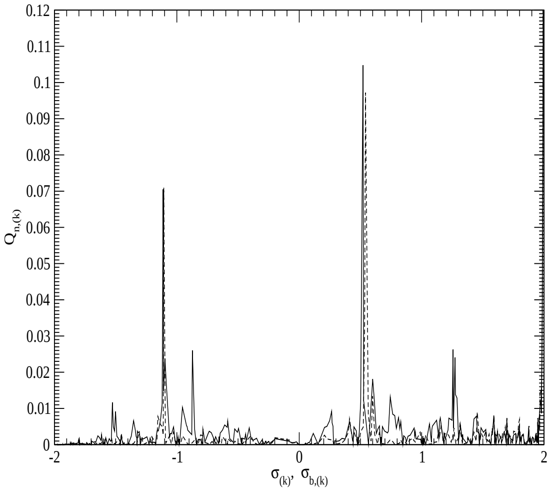

Figure 10. The overlap integrals $Q_{n,k}$ are shown for two models of the planet: the model without the phase transition - dashed curve, and the original model with the phase transition - solid curve.

of these numerical features depends on the number of trial functions j_{max} decreasing with increase of j_{max}. Similar to the case of a polytropic star with index 1.5 (PI), there are two 'global' modes with large values of the overlap integrals, with $\bar{\sigma}_{(1)} \approx 0.5$ and $\bar{\sigma}_{(2)} \approx -1.1$. The frequencies and amplitudes of these modes depends only weakly on the number of trial functions, and these modes are especially important for the problem on hand. However, contrary to the case of a polytropic star with index 1.5, there are some other markedly large values of $Q_{(k)}$ associated with modes at other eigenfrequencies (eg. near $\sigma_3 \approx -0.9$ and $\sigma_4 \approx 1.25$). These can also be associated with global modes, which are, however, less stable

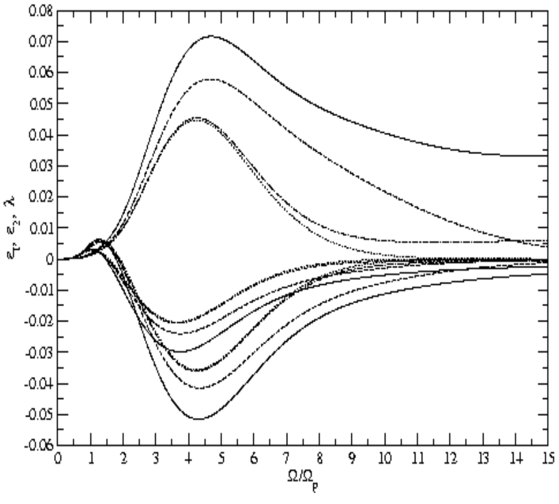

Figure 11. Same as Figures 7 and 9, but now the dotted and dashed curves are calculated with using the binned overlap integrals corresponding to the global modes. We take into account only the two 'main' global modes to calculate the dotted curve and the eight global modes discussed in the text to calculate the dashed curve. The dot-dashed curve is calculated using the overlap integrals corresponding to the model without the phase transition. Note the dotted and dot-dashed curves for ϵ_I and λ practically coincide.

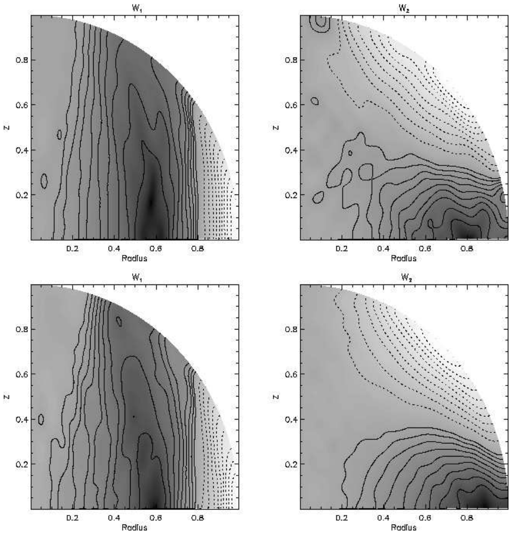

Figure 12. The distribution of $W_{(k)}$ over the planet. $W_{(k)} = 0$ at the origin. Contour lines of different style correspond to values of W_k of opposite signs (which are always found to occur). Ten contour levels of W_n (n=1,10) for each sign are defined as follows: $W_n = \frac{1}{n} W_*$, where W_* is one of the maximum or minimum value of $W_{(k)}$. The upper left (right) plot corresponds to the main global mode W_1 with $\sigma_1 = 0.521$ (W_2 with $\sigma_2 = -1.11$). The lower left and right plot show the same distributions but calculated for the planet model without the phase transition.

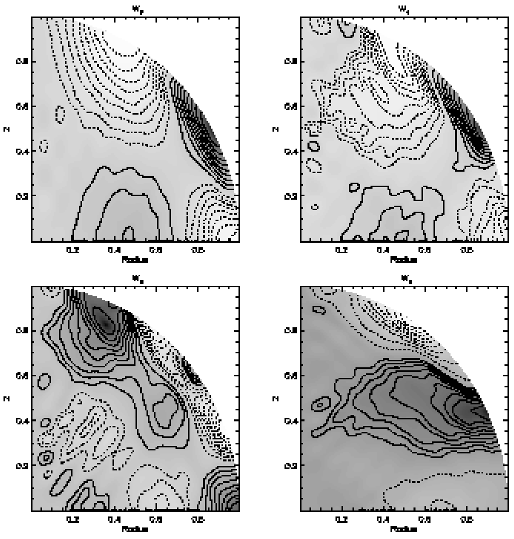

Figure 13. Same as Fig. 12 but for W_3 with $\sigma_3 = 0.873$ (upper left plot); W_4 with $\sigma_4 = 1.257$ (upper right plot); W_5 with $\sigma_5 = 1.273$ (lower left plot); W_6 with $\sigma_6 = -1.525$ (lower right plot).

with respect to changes of j_{max}. They cannot be reliably identified with a small number of the trial functions ($j_{max} = 25$ in our case). We discuss properties of these modes later in this section.

In Figure 7 we show the quantities ϵ_2, λ and ϵ_I defined by equations (69-71) which determine the energy and angular momentum transfer through equations (68) and (72). As for figure 6 the curves of different types correspond to different values of j_{max}. It is seen from this Figure that when $\bar{\Omega}$ is sufficiently large the curves representing large values of $j_{max} = 100$ and 225 are in a very good agreement with each other. The curves representing ϵ_I and λ for $j_{max} = 25$ are also in qualitative agreement with those corresponding to the larger value of j_{max}. However, the curve representing ϵ_2 deviates significantly when $\bar{\Omega} > 7$. When $\bar{\Omega}$ is small, the curves representing $j_{max} = 25$ and 100 have larger values compared to the case with $j_{max} = 225$. This is due the contribution of spurious modes with eigenfrequencies very close to $\sigma = 2$. In principle, we can improve the agreement between different curves significantly simply by discarding these modes. However, as we will see below it is possible to improve the stability of our numerical scheme with respect to the choice of different numbers of trial functions and suppress the influence of these spurious modes automatically.

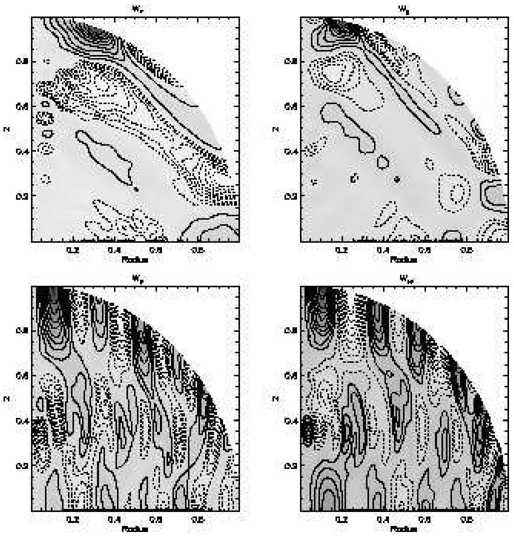

Figure 14. As in Fig. 12 but here we show the distributions of W_7 with $\sigma_7 = -1.5$ in the upper left plot and W_8 with $\sigma_8 = -1.353$ in the upper right plot. Two non-global modes showing small scale structure with $\sigma_9 = 0.49$ (lower left plot) and $\sigma_{10} = -0.5$ (lower right plot), are also shown.

5.3.1 Binned eigenfrequencies and overlap integrals

In order to improve the stability of our numerical scheme with respect to numerical noise we would like to separate the eigenspectrum into bins with a finite frequency width and adopt the sum of the overlap integrals within a particular bin instead of $Q_{(k)}$. To begin, we redefine the overlap integral according to the rule

$$Q_{n,(k)} = \bar{\sigma}^2_{(k)} \sqrt{(4 - \bar{\sigma}^2_{(k)})} Q_{(k)}. \tag{95}$$

It follows from equation (69), that the quantity ϵ_2 has especially simple form when expressed in terms $Q_{n,(k)}$, namely

$$\epsilon_2 = C_2 \bar{\Omega}^4 \sum_{(k)} Q^2_{n,(k)} I^2_{2,-m}(y_k). \tag{96}$$

To define the frequency bins let us separate the eigenspectrum into regions between successive minima of $Q^2_{n,(k)}$ and treat all $Q_{n,(k)}$ and $\sigma_{(k)}$ within such a region as belonging to the same bin. Note that modes defining minima are not included in the bins. Accordingly, we have

$$Q_{b,(l)} = \sqrt{\sum Q^2_{n,(k)}}, \quad \sigma_{b,(l)} = \frac{(\sum Q^2_{n,(k)}\sigma_{(k)})}{Q^2_{b,(l)}}, \tag{97}$$

as new 'binned' overlap integrals and 'binned' eigenfrequencies. Here, the summation is performed over all eigenfrequencies belonging to the same bin, and l is a number of a bin [5].

The result of comparison between the 'binned' quantities $Q_{b,k}$ corresponding to different j_{max} and the quantities $Q_{n,k}$ calculated with the largest $j_{max} = 225$ is shown in Figure 8. One can see from this Figure that the binned quantities calculated for $j_{max} = 100$ and $j_{max} = 225$ are in a good agreement. The results corresponding to $j_{max} = 25$ agree with what is shown for larger values of j_{max} for the two 'main' global modes. They are also in qualitative agreement for $\sigma_{(k)} < 0$, but deviate in a part of the spectrum with positive values of $\sigma_{(k)}$. It turns out that this deviation is not important for our purposes. Indeed, the positive part of the spectrum plays a role in the tidal response problem when $\bar\Omega$ is small. In this case width of the function $I_{2,-2}(y)$ is rather large, and the tidal response is mainly determined by the 'main' global mode with $\bar\sigma_1 \approx 0.5$ and the largest overlap integral. When $\bar\Omega$ is large, the tidal response is mainly determined by the modes with negative $\sigma_{(k)}$ which can then comove with the tidal perturbation near periastron. The width of $I_{2,-2}(y)$ decreases with increase of $\bar\Omega$, and, when the rotation rate is large, the tidal response is determined by several modes with sufficiently large overlap integral and sufficiently large absolute values of $\sigma_{(k)}$. This effect explains in part why the energy transfer in the rotating frame determined by the quantity ϵ_2 tends to some non-zero value with increase of the rotation rate (see e.g. Figure 7 and Figure 9).

In Figure 9 we show the quantities ϵ_I, ϵ_2 and λ calculated using the binned overlap integrals for the different values of j_{max} and the corresponding quantities calculated using the non-binned overlap integrals with $j_{max} = 225$. Comparing Figure 7 with Figure 8 we see that the use of the binned quantities does allows us to improve significantly the stability of our numerical scheme with respect to different numbers of basis functions. Now, all curves are in a good agreement with each other for the whole considered range of $\bar\Omega$.

5.3.2 Eigenspectrum of the model without the phase transition

In Figure 10 we show the result of calculation of the overlap integrals for the model with 'smoothed out' phase transition (dashed curve) together with the overlap integrals for the model with the phase transition. As it is seen from this Figure the two 'main' global modes have practically the same overlap integrals for the both models. However, other prominent spikes present in the model with a phase transition are absent for the model without the phase transition. Therefore, there only two global modes in that case. One can assume that the presence of the other global 'non standard' modes in the realistic planet models is related to the presence of the phase transition. In fact, as we will see below these modes are also present in the planet models with larger radii where the phase transition is absent. It is reasonable to suppose that the presence of some of these modes is related to a sharp decrease of the density after the radius of the phase transition (or the melting point for the models with larger radii, see Figures 3 and 4) in the realistic planet models.

---

[5] Note that this procedure is not unique, and better results may be achieved with a more sophisticated scheme of binning. However, our procedure is, perhaps, the simplest one, and it is definitely sufficient for our purposes.

5.3.3 Global modes

As we have pointed out above there is a set of modes characterised by relatively large values of the overlap integrals. These modes are referred to as global modes. Physically, these modes have eigenfunctions for which $W_{(k)}$ varies on a large scale. In this situation, the overlap integrals are not averaged to small values after integration over the volume of the planet.

As can be seen from Figures 6, 8 and 10 there are more than ten modes with markedly large overlap integrals. However, they are not equally important for the problem on hand. The two most important modes are 'the main' global modes with the largest values of the overlap integrals. These are present in all our models as well as in polytropic stars. Other global modes with negative values of $\sigma_{(k)}$ can also play an important role in the tidal response. Additionally, it is interesting to consider the positive and negative frequency global modes with the largest values of $Q_{n,(k)}$ after the main modes. These modes contain information about the difference of the realistic planet models from over-simplified polytropes, and may be of interest for another problems as well. There are eight modes satisfying these criteria. Their eigen frequencies and overlap integrals are shown in Table 1. W_1 and W_2 are the two 'main' global modes. W_4 and W_5 as well as W_6 and W_7 have very close eigen frequencies. Most probably, these modes are doublets split as a result of a perturbation.

In Figure 11 we show the quantities ϵ_I, ϵ_2 and λ calculated with only two global modes (the dotted curves), with the eight global modes (the dashed curves), and with the whole spectrum of modes (the solid curves). The dot-dashed curves represent the corresponding

Table 1. The eigen frequencies and overlap integrals of the global modes.

$W_{(k)}$	$\sigma_{(k)}$	$\sigma_{b,(k)}$	$Q_{n,(k)}$	$Q_{b,(k)}$
W_1	0.521	0.521	0.105	0.1065
W_2	-1.11	-1.11	0.07	0.072
W_3	-0.873	-0.872	0.026	0.026
W_4	1.257	1.257	0.026	0.026
W_5	1.273	1.276	0.024	0.03
W_6	-1.526	-1.525	0.0117	0.0127
W_7	-1.5	-1.5	0.0091	0.0096
W_8	-1.353	-1.349	0.0066	0.0085

quantities calculated for the model without the phase transition. One can see that the curves for the model without the phase transition are very close to the curves calculated using only the two 'main' global modes - the result expected from our previous discussion. In general, the curves calculated using the global modes give a good approximation to the curves calculated with help of the whole spectrum excepting the curves representing the transfer of energy in the inertial frame, ϵ_2 at a high rotation rate, $\bar{\Omega} > 10$. The solid curve determined by the whole spectrum gives much larger energy transfer in this case. This is due to the influence of the modes with eigen frequencies very close to -2. It is not clear whether this effect is physical or it is determined by numerical inaccuracies of our method. A calculation with significantly larger number of the trial functions may resolve this question. However, this effect is unimportant for our purposes and will not be discussed further.

In Figures 12-14 we show the distribution of W_k over the planet for the eight global modes. Additionally, in Figure 14 we show the distribution of W_k for two 'non-global' modes: W_9 with $\sigma_9 = 0.49$ and W_{10} with $\sigma_{10} = -0.5$. These modes have very small overlap integrals. In the upper panels of Figure 12 the two 'main' modes W_1 and W_2 are shown, and in the lower panels of the same Figure we show the same modes calculated for the model without the phase transition. One can see that these modes have essentially the same structure for the both models. Moreover, these distributions are very similar to the distributions of the corresponding modes for the case of a $n = 1.5$ polytrope (IP). Therefore, it is natural to suggest that the dependence of the structure of the 'main' modes on the structure of a planet is rather insignificant (see also Figures 19 and 23 below). Other global modes have structures with amplitudes that are more concentrated towards the boundary of the planet when compared to the 'main' modes. It is instructive to compare the global and non-global modes. One can see from Figure 14 that the non-global modes are characterised by a large number of patterns with alternating signs. These patterns give compensating contributions to the overlap integrals thus significantly decreasing their values.

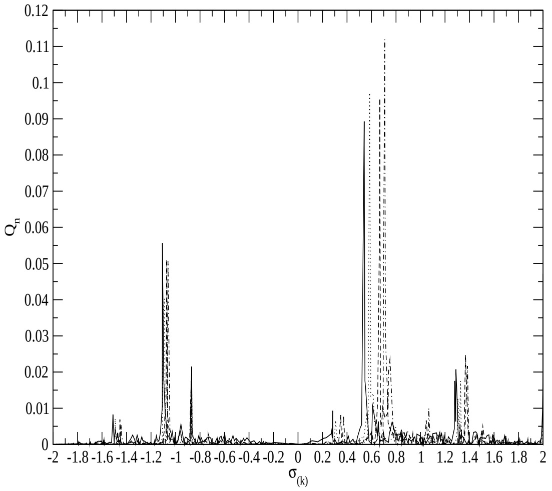

Figure 15. The overlap integrals $Q_{n,(k)}$ are shown for the planet models with $M_* = 1M_J$, and four different radii: $R_* = 1.2R_J$ (solid curve), $R_* = 1.4R_J$ (dotted curve), $R_* = 1.8R_J$ (dashed curve), and $R_* = 2R_J$ (dot-dashed curve).

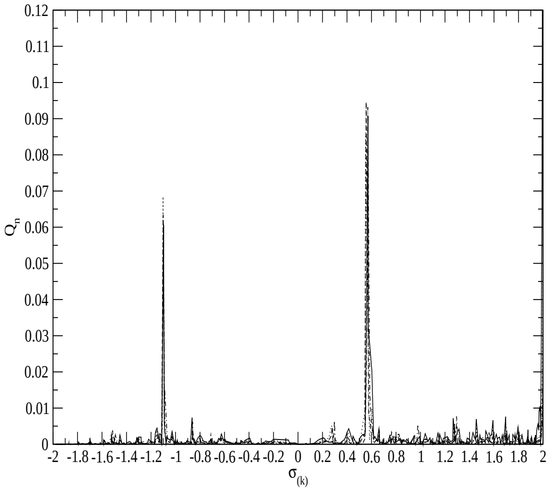

Figure 16. The same as Fig. 15 but for $M_* = 5M_J$. The solid, dotted, dashed and dot-dashed curves are for $R_* = 1.03R_J$, $1.4R_J$, $1.6R_J$ and $2R_J$, respectively.

5.4 Eigenspectra of the planets with larger masses and radii

In Figure 15 we show the dependency of the overlap integral $Q_{n,(k)}$ on the eigenfrequency $\sigma_{(k)}$ for the planet models with planet mass equal to the mass of Jupiter with four different radii, $R_* = 1.2R_J$, $1.4R_J$, $1.8R_J$ and $2R_J$. The general structure of the spectrum is close to that of the planet with $M_* = 1M_J$, and $R_* = 1R_J$, see (Figure 8). In all cases there are the two 'main' global modes. Also there are some other 'non-standard' global modes with eigenfrequencies close to the corresponding eigenfrequencies of the model with $R_* = 1R_J$. The 'main' modes slightly change their position with growth of planet radius, and their

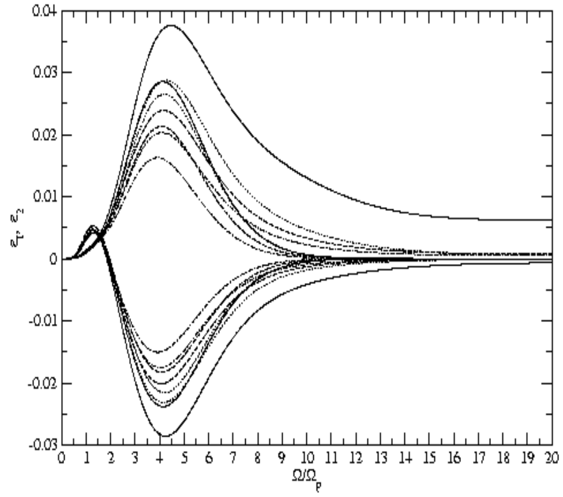

Figure 17. The dependence of ϵ_I and ϵ_2 for the planet models with $M_J = 1M_*$ and $R_* = 1.2R_J$ (solid curves), $R_* = 1.4R_J$ (dotted curves), $R_* = 1.8R_J$ (dashed curves), and $R_* = 2R_J$ (dot-dashed curves). The curves which always pass through positive values correspond to ϵ_2. The curves of the same type with smaller amplitude correspond to ϵ_I and ϵ_2 calculated using only the two 'main' global modes.

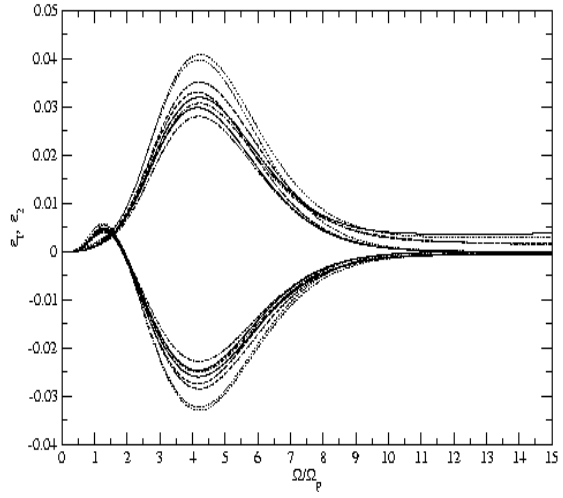

Figure 18. The same as Fig. 17 but for $M_* = 5M_J$. The solid, dotted, dashed and dot-dashed curves are for $R_* = 1.03R_J$, $1.4R_J$, $1.6R_J$ and $2R_J$, respectively.

overlap integrals also slightly depend on the radius, being however rather close to each other. It is interesting to point out that the overlap integrals corresponding to the 'non-standard' global modes are smaller than those corresponding to the model with $M_* = 1M_J$, and and $R_* = 1R_J$. Therefore, the influence of the 'main' global modes on the energy transfer is more pronounced than in that case (see Figure 17).

Table 2. The binned eigen frequencies and overlap integrals of the main modes for $M_* = 1M_J$.

R_*/R_{pl}	1.2	1.4	1.8	2
$\sigma_{b,1}$	0.54	0.58	0.65	0.71
$Q_{b,1}$	0.093	0.097	0.117	0.12
$\sigma_{b,2}$	-1.1	-1.09	-1.076	-1.037
$Q_{b,2}$	0.057	0.06	0.054	0.051

Table 3. The binned eigen frequencies and overlap integrals of the main modes for $M_* = 5M_J$.

R_*/R_{pl}	1.03	1.4	1.6	2
$\sigma_{b,1}$	0.55	0.53	0.57	0.59
$Q_{b,1}$	0.1	0.105	0.098	0.096
$\sigma_{b,2}$	-1.1	-1.1	-1.1	-1.1
$Q_{b,2}$	0.061	0.069	0.064	0.058

In Figure 16 we show the results of calculations for models which have $M_* = 5M_J$ with $R_* = 1.03R_J$, $1.4R_J$, $1.6R_J$ and $2R_J$. As seen from this Figure the spectrum is quite stable for this case, such that the curves corresponding to different planet radii can be hardly distinguished from each other. Also, the spectrum is totally dominated by the two 'main' global modes with $\sigma_1 \approx 0.55$ and $\sigma_2 \approx -1.1$. In fact, for these models it is possible to identify reliably only three non-standard global modes with $\sigma_{(k)} \approx -0.85$, 0.3 and 1.3. These modes, however, have rather small overlap integrals.

In Figures 17 and 18 we show the dependence of the quantities ϵ_I and ϵ_2 which determine the energy transfer in the inertial and rotating frames, respectively, on $\bar{\Omega}$ for the set of planet model considered in this Section. Also, we compare these quantities with the same quantities calculated using only the two 'main' global modes and the 'binned' overlap integrals and eigenfrequencies discussed above. The corresponding eigenfrequencies and overlap integrals are shown in Tables 2 and 3.

In Figure 17 we show the results of calculations for the planet models with $M_* = 1M_J$ and in Figure 18 the case of $M_* = 5M_J$ is shown. As seen from these Figures, the quantities determined by using only the two 'main' modes give a good approximation for all curves excepting the cases of the planet models that have $M_* = 1M_J$ with $R_* = 1.2R_J$ and $M_* = 5M_J$ with $R_* = 1.03R_J$. In those cases the curves giving ϵ_2 deviate significantly when $\bar{\Omega}$ is large.

Figures 19-23 illustrate the effects of changing planet radius and mass on the form of $W_{(k)}$, for the global modes.

In Figure 19 we show the distributions for the two 'main' global modes W_1 and W_2 in the case of the planets with $M_* = 1M_J$ and radii larger than the radius of Jupiter. Comparing

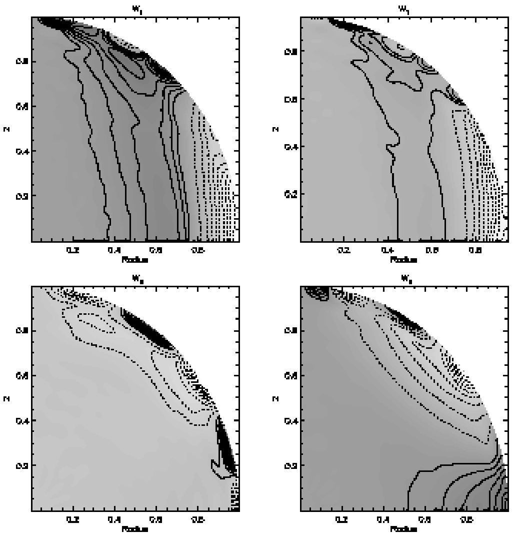

Figure 19. The distribution of $W_{(k)}$ for $M_* = 1M_J$ with two different radii $R_* = 1.4R_J$ and $R_* = 2R_J$. The two 'main' global modes W_1 (upper panels) and W_2 (lower panels) are shown with the left (right) plots corresponding to $R_* = 1.4R_J$ ($R_* = 2R_J$). The upper left (right) plot corresponds to $\sigma_1 = 0.58$ with $Q_{n,1} = 0.097$ ($\sigma_1 = 0.71$ with $Q_{n,1} = 0.11$). The lower left (right) plot corresponds to $\sigma_2 = -1.1$ with $Q_{n,2} = 0.038$ ($\sigma_2 = -1.06$ with $Q_{n,2} = 0.051$).

this Figure and Figure 12 we see that the spatial structure of the 'main' global modes only slightly changes with change of planet radius. These modes may be considered as 'stable' modes with respect to changes of this parameter. In Figure 20 we show the influence of changing radius on the 'non standard' global mode W_3 with $\sigma_3 \approx -0.9$. The distribution of this mode is practically the same for planet radii in the range $1.2R_J - 2R_J$, and therefore this mode is particularly 'stable'. Examples of 'non-stable' modes are shown in Figures 21 and 22. We plot the mode W_4 with $\sigma_4 \approx 1.3$ in Figure 21 and the mode W_5 with $\sigma_5 \approx -1.5$ in Figure 22. One can see from these Figures that the region with non-negligible $W_{(k)}$ is gets smaller with radius. Accordingly, the overlap integrals get smaller as well, see Figure 15.

As follows from Figure 16 the effective spectra of the models with $M_* = 5M_J$ is pretty stable with respect to a change of radius, and the overlap integrals corresponding to the 'non standard' global modes are small compared with those corresponding to the 'main' global modes. Therefore, in Figure 23 we show only the two 'main' global modes for $R_* = 1.03R_J$ and $R_* = 2R_J$. The general structure of the modes is similar to the case $M_* = 1M_J$ (see Figures 12 and 19). However, there is an interesting feature of the distributions in the

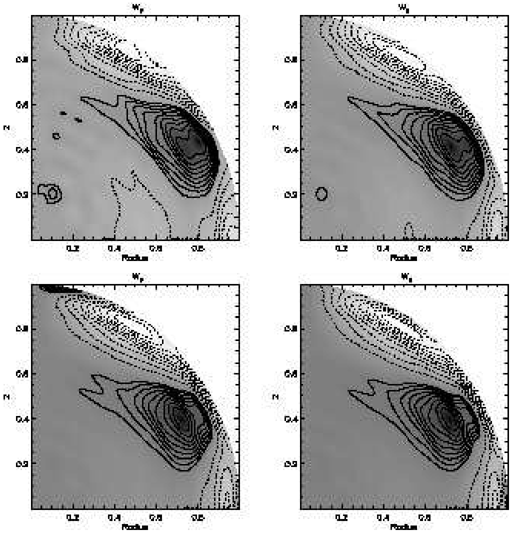

Figure 20. The form of the 'non standard' global mode W_3 with $\sigma_3 \approx -0.9$ for the planet models with $M_* = 1M_J$ and four different radii: $R_* = 1.2R_J$, upper left plot; $1.4R_J$, upper right plot; $R_* = 1.8R_J$ lower left plot; $R_* = 2R_J$, lower right plot.

case $R_* = 1.03R_J$. In this case a small scale pattern is superimposed on the large scale distributions of W_1 and W_2. Most probably, this effect can be explained by mixing between these two global modes and neighbouring local modes as a result of a perturbation.

6 ROTATION RATE AND ENERGY EXCHANGE IN THE STATE OF PSEUDO-SYNCHRONISATION

When the state of pseudo synchronisation is maintained with the value of the angular velocity being equal to its equilibrium value Ω_{eq}, the angular momentum transfer is absent $\lambda(\Omega_{eq}) = 0$. In this case the energy transfer in the inertial frame is equal to the energy transfer in the rotating frame, and therefore the corresponding curves in Figures 9, 11, 17 and 18 intersect each other. One can see from these Figures that the intersection point have similar coordinates for all models we consider, and therefore the dimensionless rotation rate $\bar{\Omega}_{eq}$ and the quantity ϵ_* determining the energy exchange through equation (74) only slightly depend on the parameters of the planet models. We summarise results of calculations of these quantities in Tables 4 and 5.

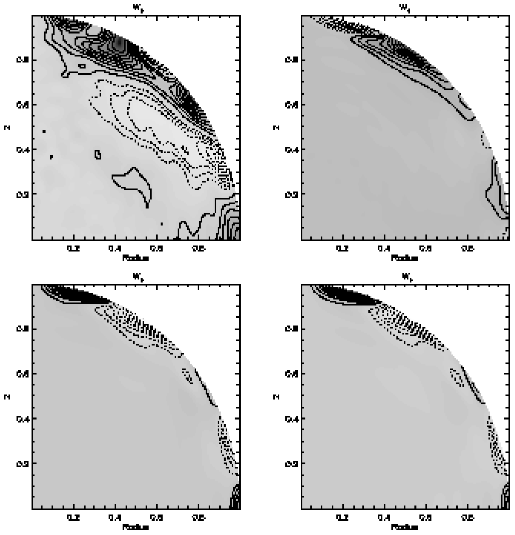

Figure 21. Same as Fig. 20 but for the global mode W_4 with $\sigma_4 \approx 1.3$.

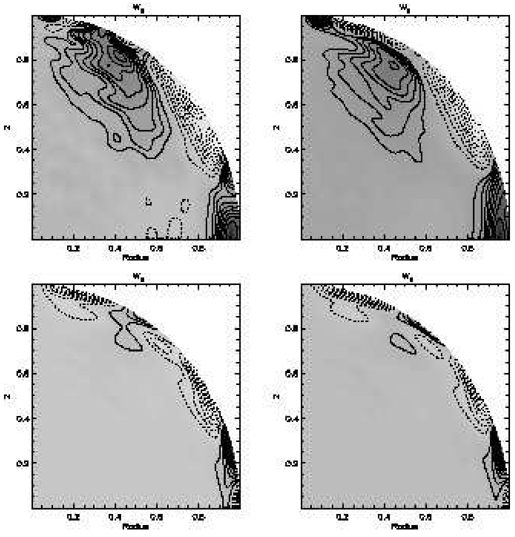

Figure 22. Same as Fig. 20 but for the global mode W_5 with $\sigma_5 \approx -1.5$.

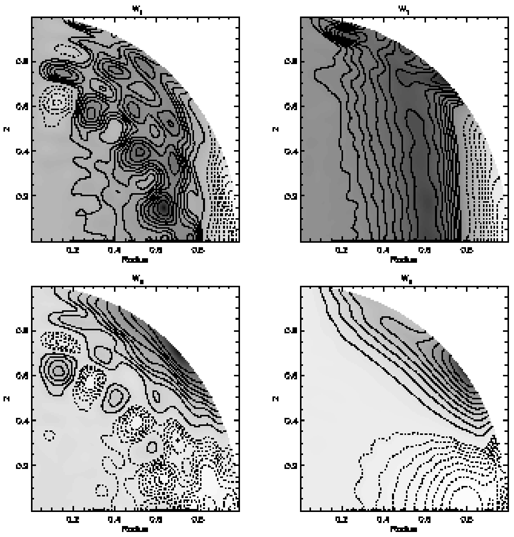

Figure 23. The same as Fig. 19 but for $M_* = 5M_J$. The two 'main' global modes W_1 (upper panels) and W_2 (lower panels) are shown with the left (right) plots corresponding to $R_* = 1.03R_J$ ($R_* = 2R_J$). For the upper plots $\sigma_1 \approx 0.57$ and $Q_{n,1} \approx 0.09$ For the lower plots $\sigma_2 \approx -1.1$ and $Q_{n,2} \approx 0.06$, for the both models.

Table 4. ϵ_* and $\bar{\Omega}_{eq}$ for the planet models with $M_* = M_J$.

R_*/R_J	1	1.2	1.4	1.6	1.8	2
ϵ_*	$5.3 \cdot 10^{-3}$	$3.6 \cdot 10^{-3}$	$3.45 \cdot 10^{-3}$	$3.6 \cdot 10^{-3}$	$3.7 \cdot 10^{-3}$	$3.6 \cdot 10^{-3}$
$\bar{\Omega}_{eq}$	1.46	1.52	1.56	1.59	1.6	1.61

As follows from these table apart from the case of a planet with Jupiter mass and radius which gives a rather large value $\epsilon_* = 5.3 \cdot 10^{-3}$, the values of ϵ_* and $\bar{\Omega}_{eq}$ are rather close to each other. Therefore, in our estimates of the time scale of tidal circularisation below we will use the 'typical' values $\epsilon_* = 3.6 \cdot 10^{-3}$ and $\bar{\Omega}_{eq} = 1.55$. Accordingly, the energy transfer will be given by

$$E_{ps} = \frac{3.6 \cdot 10^{-3}}{\eta^6} E_*, \tag{98}$$

regardless of the planet radius and mass.

Table 5. ϵ_* and $\bar{\Omega}_{eq}$ for the planet models with $M_* = 5M_J$.

R_*/R_J	1.03	1.2	1.4	1.6	1.8	2
ϵ_*	$3.6 \cdot 10^{-3}$	$3.6 \cdot 10^{-3}$	$4.2 \cdot 10^{-3}$	$3.7 \cdot 10^{-3}$	$3.55 \cdot 10^{-3}$	$3.4 \cdot 10^{-3}$
$\bar{\Omega}_{eq}$	1.55	1.55	1.54	1.54	1.54	1.55

In Figure 16 we show the dependence of E_{ps} on η as a solid curve. The dotted, dashed and dot-dashed curves correspond to the energy transfer associated with the fundamental modes, E_f. They are calculated with help of equations derived in IP and presented in Appendix [6]. In a similar manner to the energy transfer associated with the inertial modes, E_f depends on the angular velocity of the planet, and we present several different curves calculated for different values of Ω. The dashed curves are calculated for a non-rotating planet with $\bar{\Omega}=0$, they correspond to a maximal energy transfer E_f^{max} as a function of Ω. The dotted curves are calculated for the case $\bar{\Omega}=\bar{\Omega}_{eq}=1.55$. The dot-dashed curves are calculated for the equilibrium angular velocity of the planet, Ω^f_{ps}, associated with the fundamental modes, see equation (A6) of Appendix. These curves give a minimal energy transfer E_f^{min} as a function of Ω, for a given η.

As follows from Appendix, in order to calculate E_f the eigenfrequencies associated with the fundamental modes, σ_f as well as the corresponding dimensionless overlap integrals, Q_f must be known. These quantities depend on the planet structure, and therefore they are different, in principle, for planets with different masses and radii, see IP for their numerical values. In Figure 16 we show the case of a planet with $M_*=M_J$ and $R_*=R_J$ (the upper dashed, dotted and dot-dashed curves), where we have $\sigma_f\approx 1.2\Omega_*$ and $Q_f\approx 0.56$. The lower dashed, dotted and dot-dashed curves represent the case of a planet with the same value of mass and $R_*=2R_J$ with $\sigma_f\approx 1.7\Omega_*$ and $Q_f\approx 0.44$. As follows from the results provided in IP, when $M_*=5M_J$ the dependence of the eigenfrequencies and overlap integrals on the planet radius is rather weak, and the corresponding energy transfer is always approximately represented by the upper dashed and dotted curves in Figure 16.

As follows from Figure 16 the inertial modes dominate the energy transfer for sufficiently large values of η. When $\bar{\Omega}=\bar{\Omega}_{eq}$ the contribution determined by the inertial waves dominates over that corresponding to the fundamental modes for $\eta>9$ in the case of $R_*=R_J$ and for $\eta>5.5$ in the case of $R_*=2R_J$. Thus, we expect that the circularisation of the planet orbits with sufficiently large periastron distances is mainly determined by the contribution associated with the inertial modes.

---

[6] Note a misprint made in (IP). Their equations (60), (61) and (64) must by multiplied by factor π^2. This has no influence on the conclusions of IP. The correct expressions are shown in Appendix.

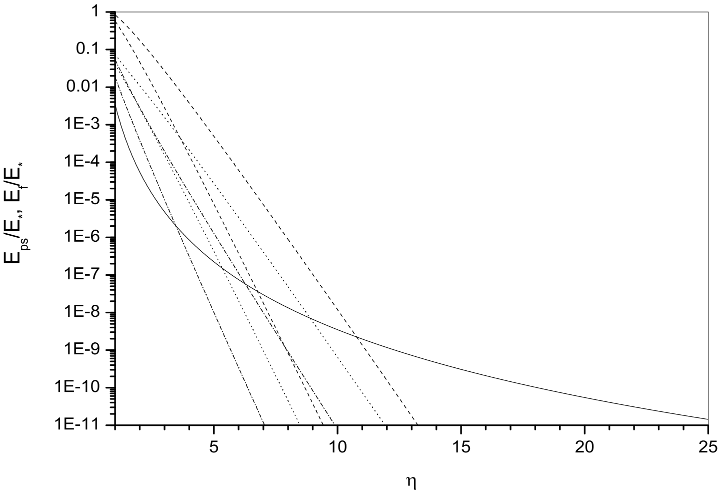

Figure 24. The energy transfer associated with the inertial modes (the solid curve) as well as the energy transfer associated with the fundamental modes as a function of the parameter η. The dashed, dotted and dot-dashed curves correspond to $\Omega = \Omega_{eq}$, $\Omega = 0$ and $\Omega = \Omega_{ps}^{f}$, respectively. Upper (lower) curves of the same type corresponds to a planet with $M_* = M_J$ and $R_* = R_J$ ($R_* = 2R_J$).

7 TIME SCALE OF ORBITAL CIRCULARISATION

In this Section we apply the results developed in the previous Sections to estimate the effect of tides exerted by the central star on the planet on the planet orbital evolution. We assume that the state of pseudo-synchronisation with $\bar{\Omega} = \bar{\Omega}_{ps} \approx 1.55$ is maintained in a situation when the inertial modes dominate over the fundamental modes in tidal response.

Apart from the fact that we mainly consider the effects of inertial waves, the formulation of the problem is analogous to what was discussed in IP. Let us consider a planetary system consisting of a few massive planet and a central star and assume that a certain planet has lost a significant amount of its orbital angular momentum, most probably due to gravitational interaction with other planets in the planetary system. Such situations have been frequently observed in numerical simulations of gravitationally interacting planets (Papaloizou & Terquem 2001, Adams & Laughlin 2003). The orbital semi-major axis of this planet, in this case, could be of the order of its 'typical' value $1 - 100Au$ while the periastron distance r_p could be very small, of the order of a few stellar radii. For a such eccentric orbit the orbital angular momentum per unit of mass is related to the periastron distance as $L_{orb} \approx \sqrt{2GMr_p}$.

If we assume that the orbital evolution is determined by tides, the angular momentum is approximately conserved while the semi-major axis may decrease due to transfer of the orbital energy into oscillations of the planet by tides and subsequent dissipation. Then, the energy may be radiated away from the planet. The conservation of the angular momentum leads to the well known fact that the radius a 'final' circular orbit, r_f is twice as large as the periastron distance r_p. Therefore, r_p can be related to the observed orbital period of the planet after circularisation, $P_{obs} = 2\pi\sqrt{(r_f^3/GM)}$, as

$$r_p = \frac{r_f}{2} = 4.36(P_3)^{2/3}\left(\frac{R_\odot}{R_s}\right)R_s, \tag{99}$$

where $P_3 = P_{obs}/(3days)$, R_s is the stellar radius and $R_\odot = 7 \cdot 10^{10} cm$ is the radius of the Sun. We have, accordingly, from equation (63)

$$\eta = 9.1\eta_0\left(\frac{R_\odot}{R_s}\right)^{3/2}P_3, \quad \eta_0 = \sqrt{\frac{M_*}{M}\frac{R_s^3}{R_*^3}}. \tag{100}$$

For the planet and the star with Jupiter and solar values of mass and radius, respectively, $\eta_0 \approx 1$.

Let us consider the evolution of the semi-major axis of the eccentric planet orbit due to tidal interactions near the orbit periastron. We can assume that the contributions from each of successive impulsive energy transfer can be added to each other only when one of two conditions is fulfilled: either the energy is dissipated during two successive periastron passages or the condition for the stochastic instability (84) is satisfied. In the latter case the evolution of the semi-major axis is stochastic, and we assume below that, in this case, our evolution equations are written for averaged over some distributions values of the corresponding quantities.

Under these assumption we can write the evolution equation for semi-major axis, $a(t)$, in the form (IP)

$$\frac{\dot a_{10}}{a_{10}} = -\frac{1}{t_{10}(t)\sqrt{a}_{10}}, \tag{101}$$

where $a_{10} = a/(10Au)$. The characteristic evolution time

$$t_{10} = 7.4 \cdot 10^8\left(\frac{MM_J}{M_\odot M_*}\right)\left(\frac{R_*}{R_J}\right)\left(\frac{10^{-9}}{\epsilon_{DT}}\right)yr. \tag{102}$$

depends on the energy transfer due to dynamic tides associated with the inertial and fundamental modes in the planet, E_{ps} and E_f, respectively, and also on the transfer of the orbital energy into stellar oscillations determined by dynamic tides exerted on the star

$$\epsilon_{DT} = \frac{(E_{ps} + E_f + E_s)}{E_*}, \tag{103}$$

where E_{ps} is given by equation (98) and E_s stands for the energy transfer associated with dynamic tides in the star. Note that the time t_{10} implicitly depends on time t through dependence of the planet radius R_* on time due to the evolutionary cooling and a possible tidal heating of the planet.

Equation (102) can be integrated to give

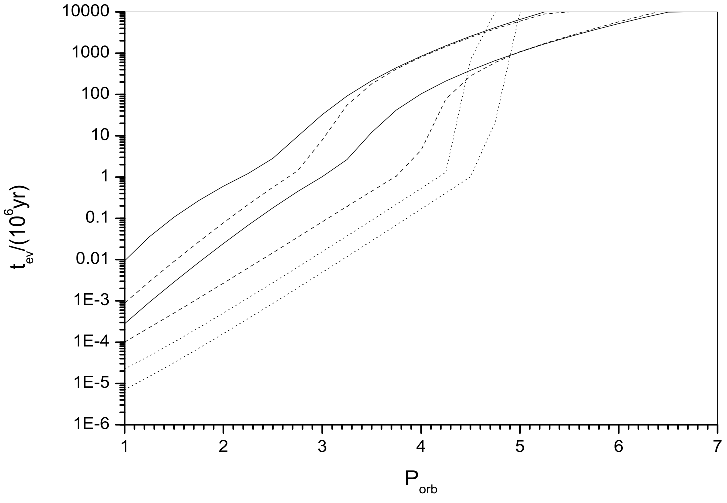

Figure 25. The circularisation time scale t_{ev} (in units of $10^6 yr$) for $1M_J$ as a function of the planet orbital period after the stage of tidal circularisation, P_{orb} (in units of days). The solid curves correspond to t_{ev} determined solely by the inertial modes. The dashed curves are calculated with help of the sum of contributions corresponding to the inertial modes, the fundamental modes and the modes excited in the star. The energy transfers determined by the inertial and fundamental modes are given by expressions corresponding to rotation of the planet at the equilibrium angular velocities Ω_{ps} and Ω^f_{ps}, respectively. The dotted curves correspond to the case of a non-rotating planet. Accordingly, the contribution of inertial modes is not taken into account. The lower (upper) curves of the same type correspond to $a_{in} = 1$ $[a = 10Au]$ ($a_{in} = 10$ $[a = 100Au]$).

$$a_{10}(t) = a_{in} \left(1 - \frac{1}{2\sqrt{a}_{in}} \int_{t_{in}}^{t} \frac{dt'}{t_{10}(t')}\right)^2, \tag{104}$$

where $a_{in}(t_{in})$ is the 'initial' value of the semi-major axis expressed in units of $10Au$. A more accurate compared to (102) definition of the evolution time scale, t_{ev}, can be obtained from equation (104) requiring that the semi-major axis a_{10} is formally equal to zero when $t = t_{ev}$. Thus

$$\frac{1}{2\sqrt{a}_{in}} \int_{t_{in}}^{t_{ev}} \frac{dt'}{t_{10}(t')} = 1. \tag{105}$$

For a constant value of t_{10}, $t_{ev} \approx 2\sqrt{a}_{in} t_{10}$. In this case we can obtain a simple estimate of t_{ev} assuming that the transfer of energy is determined only by the inertial modes. Setting $E_s = E_f = 0$ in equation (103) and substituting equations (98), (100) and (103) into (102), we have

$$t_{ev} \sim 2 \cdot 10^8 \left(\frac{M_*}{M_J}\right)^2 \left(\frac{M}{M_\odot}\right)^{-2} \left(\frac{R_*}{R_J}\right)^{-8} P_3^6 \sqrt{a_{in}} \quad yr. \tag{106}$$

Note a very strong dependence of t_{ev} on R_* and P_{orb}.

Results of numerical calculations of t_{ev} are shown in Figure 25 for the case of a planet with $M_* = 1M_J$, and in Figure 26 for a planet with $M_* = 5M_J$. In order to calculate t_{ev} we use expressions for the energy transfer associated with the fundamental modes given in Appendix, the corresponding eigenfrequencies and overlap integrals are given in IP. The

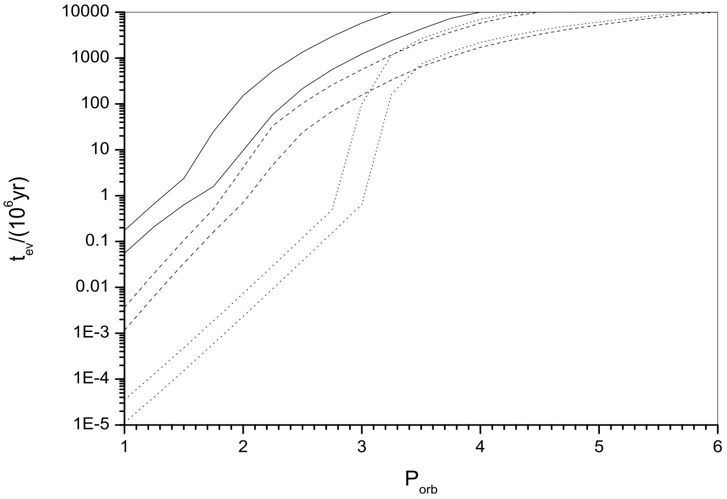

Figure 26. The same as Figure 25 but for $M_* = 5M_J$.

dependence of R_* on time is taken from Burrows et al (1997) where a cooling history of isolated planets is considered. Thus we neglect effects of tidal heating on the planet size and structure reserving their discussion for a future work. Burrows et al (1997) consider evolution of the planet radius starting from the initial time $t_{in} \sim 10^6 yr$ and until a maximal time $t_{max} \sim 10^9 yr$ is reached. We set the initial time $t_{in} = 2 \cdot 10^6 yr$. We assume that the planet radius is not changed significantly for $t > t_{max}$ and set $R_*(t > t_{max}) = R_*(t_{max})$ with $R_*(t_{max}) = 7.2 \cdot 10^9 cm$ for $M_* = M_J$ and $R_*(t_{max}) = 7.67 \cdot 10^9 cm$ for $M_* = 5M_J$. The lower curves of the same type in Figures 25 and 26 correspond to $a_{in} = 10Au$ and the upper curves are calculated for $a_{in} = 100Au$.

In Figure 25 the solid curves describe the dependence of t_{ev} on P_{orb} calculated under assumption that only inertial waves contribute to the tidal evolution, and accordingly, in this case $E_{st} = E_f = 0$ in equation (103). For the dashed curves we take into account all the contributions to the sum in (103) [7]. In order to calculate E_s we model the star as a non rotating $n = 3$ polytrope and take into account the contributions of g, f and low order p modes, see IP for details. The contribution of the fundamental modes operating in the planet, E_f is calculated for the case of rotation of the planet at the equilibrium angular velocity associated with the fundamental modes, see equation (A6) of Appendix. In this case E_f is given by equation (A7). This may be justified according to the following arguments. The inertial modes dominates over the fundamental modes at sufficiently large values of η, and accordingly at sufficiently large values of P_{orb}, and the fundamental modes dominate at smaller values of P_{orb}. Taking into account that the contribution of fundamental modes decreases exponentially with increase of P_{orb}, the transition from the case of domination of the fundamental modes to the case of domination of inertial modes occurs near a certain value of P_{orb}. Taking into account that a planet with a low value of the moment of inertia has the angular velocity always close to the equilibrium value determined by the modes dominating the energy transfer, the dashed curve could give an order of magnitude estimate of t_{ev} for the whole range of P_{orb}. The dotted curves show the results of calculation of t_{ev} for the case of a non rotating planet. In this case the energy transfer determined by the inertial modes is absent and we set $E_{ps} = 0$ in equation (103) and we use equation (A5) to calculate E_f.

---

[7] Note that conditions for the dissipation of the mode energy and the condition for the stochastic instability to set in are different for the inertial and fundamental modes in the planet and also for the modes determining the tidal response of the star. Therefore, simple adding of different contributions to the sum in (103) is, strictly speaking, not correct. However, we assume hereafter that this procedure gives correct order of magnitude estimates reported in this Paper.

As seen from Figure 25 when $M_* = 1M_J$ the inertial modes dominate for $P_{orb} > 4-4.5 days$. The time scale of circularisation is smaller than a typical life time of a planetary system $\sim 5Gyr$ when $P_{orb} < 6days$ for $a_{in} = 10Au$ and when $P_{orb} < 5days$ for $a_{in} = 100Au$. It is interesting to note that the contribution of the fundamental modes sharply decrease when $t_{ev} > 10^6 yr$. This is simply because the energy transfer associated with the fundamental modes is highly sensitive to the radius of the planet (see Appendix). It can lead to a substantial change of the semi-major axis only when the planet radius is close to its 'initial value' $R_*(t_{in}) \sim 2R_J$. The cooling of the planet results in a decrease of the planet radius on a time scale $\sim 10^6 yr$ and the contribution of the fundamental modes quickly become unimportant after this time is reached. The tides exerted on the star are not significant at all for a planet with $M_* = 1M_J$.

In Figure 26 we show the results corresponding to a planet with $M_* = 5M_J$. Contrary to the previous case now the inertial modes are not important for the whole range of P_{orb} and the circularisation time scale at large values of P_{orb} is determined by tides exerted by the planet on the star. This may be explained as follows. At large values of P_{orb} the circularisation time scale is of the order of several Gyr. A planet with its mass in the range $1M_J - 5M_J$ and its age of the order of a few Gyr has the radius close to $R_*(t_{max}) \sim 1R_J$. The circularisation time scale is mainly determined by the expressions for the energy transfer calculated for this radius. Assuming that the inertial modes dominate we can use equation (106) to estimate t_{ev}. As follows from this equation $t_{ev} \propto M_*^2$. When eg. $P_{orb} = 6days$ and $a_{in} = 10Au$ we have $t_{ev} \sim 5Gyr$ for $M_* = 1M_J$ and $t_{ev} \sim 25Gyr$ for $M_* = 5M_J$. Obviously, the inertial modes cannot lead to a significant decrease of the semi-major distance in the latter case over the life time of the planetary systems. Unlike the situation with the inertial modes, the energy transfer determined by the stellar modes grows with the planet mass, and therefore the tides exerted on the star dominate when the planet mass is sufficiently large.

8 CONCLUSIONS AND DISCUSSION

In this Paper we have developed and extended a new self-adjoint formalism for the problem of small stellar oscillations proposed in our recent paper(PI). We went on to apply this to the calculation of the tidal response of uniformly rotating fully convective planets and stars which undergo a single encounter in a parabolic orbit or a sequence of multiple encounters in a weakly bound orbit. This was then applied to the problem of the tidal circularisation of the orbits of the extrasolar planets.

In section 2 we began by showing that the general formalism, presented in PI when $W = \rho' c^2/\rho + \Psi^{int}$ is used as variable characterising linear eigenmodes, can also be applied when the Lagrangian displacement is used. The advantage of this approach is that, as no low frequency approximation is needed, it allows us to consider pulsations of arbitrary frequency. We derived general expressions for the energy and angular momentum transfer that occurs when a rotating planet or a star passes through periastron in a parabolic or highly eccentric orbit around a central mass The amplitudes and phases of the eigenmodes excited in the planet or a star as a result of the tidal encounter were also determined.

We showed that these expressions can be represented in terms of a spectral decomposition over the normal modes of the self-adjoint operator (15). We also obtained a self-consistent expression for the rate of dissipation of an excited mode to leading order in the small parameter defined by the ratio of pulsation period to a characteristic dissipation time scale.

In section 3 we focused on the case of low frequency inertial modes, showing how the more general formalism in terms of the Lagrangian displacement can be reduced to that in PI in the low frequency limit. This procedure allows one to separate out the contribution associated with the inertial modes and simplify the equations governing free pulsation of a rotating planet or a star. In that case the corresponding self-adjoint problem is formulated through equations (48) and (49). Note that the tidal response of the inertial modes to impulsive tidal forcing has not been described using other methods.

We showed in section 4 that when the rotating planet or a star approaches periastron in an unperturbed state the tidal energy and angular momentum transfered through the excitation of inertial modes are given by very simple expressions (68) and (74). We considered the multi-passage problem assuming that there was no significant dissipation of mode energy between successive periastron passages, and found a simple condition (84) for the occurrence of stochastic instability that results in the stochastic gain of inertial mode energy over many periastron passages. This was quantitatively similar to that given by IP for f modes. We found that for stochastic instability the circularisation process has to start with $a >\sim 30AU$, for final periods of ~ 3 days. or $\sim 1-2AU$ for final orbital periods ~ 1.2 days.

In section 5 we applied our formalism to fully convective rotating giant planets. In order to evaluate the expressions for the energy and angular momentum transfer the eigenspectrum of (49) must be found numerically, for a given model. We calculated the eigenspectrum of the inertial modes for several planet models with a realistic equation of state. The details and stability of the numerical method we used are discussed in section 5.2. We considered planet models with two different masses equal to $1M_J$ and $5M_J$, with radii in the range $1-2R_J$. We found that, as in the case of $n=1.5$ polytrope considered by PI, the tidal response was determined by a few 'global' eigenmodes with a large scale distribution of perturbed quantities. Two 'main' or 'standard' global modes have eigenfrequencies close to those corresponding to the $n=1.5$ polytrope. These modes have the largest overlap integrals characterising coupling between the tidal field and the eigenmodes. However, we found that for realistic planet models, there could be 'non-standard' global modes possibly related to a sharp change of structure occurring near to the point of ionisation of hydrogen. The structure of the 'non-standard' modes as well as their stability with respect to a change of the planet mass and radius was discussed.

The results obtained for the eigen spectra of realistic planet models were applied to the problem of tidal circularisation of the orbits of the extrasolar planets in sections 6 and 7. In section 6 we calculated the rotational angular velocity for which the net angular momentum transferred was zero. Because of the relative low inertia of the planet compared to the orbit it is expected to rapidly attain this angular velocity and achieve a state of pseudo synchronisation. The angular velocity associated with pseudo synchronisation was found to be always close to 1.55 times the angular velocity of a circular orbit at periastron.

Orbital evolution arises through the transfer of orbital energy to the modes of oscillation. Transfers at successive periastron passages lead to orbital circularisation. This is the case, either when the mode energy is dissipated directly between encounters, or when the system is in the regime of stochastic instability. We compared the contribution associated with the inertial modes with the contribution associated with the fundamental modes, in a state of pseudo synchronisation, to the circularisation time scale in section 7. We found that the inertial modes led to effective circularisation of a giant planet with mass $\sim 1M_J$ on a time scale smaller than or of the order of a few Gyr, when the initial semi major axis was less than $10AU$ and the final orbital period after circularisation $P_{orb} < 6 days$. In this case the inertial modes play the most important role at the longer periods. However, the inertial waves are less important for the planets of larger mass $5M_J$ that we considered. In that case the dynamic tides exerted on the star central star, which we assumed to be solar like, play a major role.

In our opinion, the most important unresolved question related to the theory discussed above is concerned with internal dissipation. Of particular concern is the internal location of modal dissipation and the related issue of whether the energy deposited can be radiated away between successive periastron passages. There are several potentially interesting channels of dissipation which may operate in our case. The non-linear parametric instability discussed by Kumar and Goodman (1996) for the case of g modes in convectively stable stars may be effective for the inertial modes as well. This instability operates when there are eigenmodes in the stars with eigenfrequencies approximately half that of the eigenfrequencies of the tidally excited modes and sufficiently large coupling coefficients. These modes may be unstable on account of parametric resonance. Taking into account that the eigenspectrum of the inertial modes is dense, unstable modes are expected to exist for sufficiently weak dissipative processes. This question will be addressed in our future work.

Our formalism is general enough that it can be extended to the case of convectively stable uniformly rotating stars and it can also be applied to other astrophysical situations where excitation of stellar pulsations with frequencies comparable to the angular velocity of rotation is important. In this particular work we assumed that the orbital and planetary angular momentum vectors were aligned. This is a very reasonable assumption when the system has many periastron passages and so readily attains a state of pseudo synchronisation during the circularisation process. However, misaligned angular momenta should be considered if the main issue is tidal capture, as in globular clusters, because in that case there is no reason for the initial angular momentum vectors to be correlated. These issues and extensions of the formalism will be considered in future work.

ACKNOWLEDGEMENTS

We are grateful to G. Ogilvie for discussions. PBI has been supported in part by RFBR grant 04-02-17444.

REFERENCES

Adams, F. C., Laughlin, G., 2003, Icarus, 163, 290

Bodenheimer, P., Pollack, J. B., 1986, Icarus, 67, 391

Burrows, A., Marley, M., Hubbard, W. B., Lunine, J. L., Guillot, T., Saumon, D., Freedman, R., Sudarsky, D., Sharp, C., 1997, ApJ, 491, 856

Friedman, J. L., Schutz, B. F., 1978, ApJ, 221, 937

Ivanov, P., Papaloizou, J., 2004, MNRAS, 347, 437 (IP)

Kochanek, C. S., 1992, ApJ, 385, 604

Kumar, P., Goodman, J., 1992, ApJ, 385, 604

Mardling, R. A., 1995, ApJ, 450, 722

Mardling, R. A., 1995, ApJ, 450, 732

Ogilvie, G. I., Lin, D. N. C., 2004, ApJ, 610, 477

Papaloizou, J. C. B., Ivanov, P. B., 2005, MNRAS, 364L, 66 (PI)

Papaloizou, J. C. B., Pringle, J. E., 1981, MNRAS, 195, 743 (PP)

Papaloizou, J. C. B., Terquem, C., 2001, MNRAS, 325, 221

Press, W. H., Teukolsky, S. A., 1977, ApJ, 213, 183 (PT)

Saumon, D., Charbrier, G., Van Horn, H. M., 1995, ApJ Suppl, 99, 713

Saumon, D., Guillot, T., 2004, ApJ, 609, 1170

APPENDIX A: ENERGY AND ANGULAR MOMENTUM TRANSFER ASSOCIATED WITH THE FUNDAMENTAL MODES

Here we show the expressions for energy and angular momentum transfer associated with the the fundamental modes in the limit $\eta \to \infty$ (IP). For the energy transfer we have

$$E_f = \frac{16\sqrt{2}}{15}\pi^2 \tilde{\sigma}_f^3 Q_f^2 \eta e^{-\frac{4\sqrt{2}}{3}\tilde{\sigma}+\eta} F_1(\tilde{\Omega}) E_*, \tag{A1}$$

and for the angular momentum transfer we have

$$L_f = \frac{32\sqrt{2}}{15}\pi^2 \tilde{\sigma}_f^2 Q_f^2 \eta e^{-\frac{4\sqrt{2}}{3}\tilde{\sigma}+\eta} F_2(\tilde{\Omega}) L_*, \tag{A2}$$

where

$$F_1(\tilde{\Omega}) = 1 + \frac{3}{2^6(\tilde{\sigma}_f \eta)^2} e^{\frac{8\sqrt{2}}{3}\beta\tilde{\Omega}\eta} + \frac{9}{2^{14}(\tilde{\sigma}_f \eta)^4} e^{\frac{16\sqrt{2}}{3}\beta\tilde{\Omega}\eta} \tag{A3}$$

and

$$F_2(\tilde{\Omega}) = 1 - \frac{9}{2^{14}(\tilde{\sigma}_f\eta)^4} e^{\frac{16\sqrt{2}}{3}\beta\tilde{\Omega}\eta}. \tag{A4}$$

$\tilde{\sigma}_f = \sigma_f/\Omega_*$ and $\tilde{\Omega} = \Omega/\Omega_*$ are the dimensionless eigenfrequency and dimensionless angular velocity of the planet, respectively and $\tilde{\omega}_+ = \tilde{\sigma}_f + 2\beta\tilde{\Omega}$. The dimensionless quantity β determines the frequency splitting of the mode due to rotation, it is close to 0.5 for our models (see IP and references therein). Q_f are the dimensionless overlap integrals, see PT and IP. When $\Omega = 0$ the energy transfer as a function of $\tilde{\Omega}$ is maximal,

$$E_f^{max} \approx \frac{16\sqrt{2}}{15}\pi^2\tilde{\sigma}_f^3 Q_f^2 \eta e^{-\frac{4\sqrt{2}}{3}\tilde{\sigma}_f\eta} E_*. \tag{A5}$$

Assuming that the fundamental modes dominate the tidal response, the state of pseudo-synchronisation is determined by condition $L_f(\tilde{\Omega}^f_{ps}) = 0$. In this case we obtain from equation (A4)

$$\Omega^f_{ps} = \frac{3}{4\sqrt{2}\beta\eta} \ln\left(\sqrt{\frac{2}{3}} 8\sigma_f\eta\right). \tag{A6}$$

When $\tilde{\Omega} = \tilde{\Omega}^f_{ps}$ the energy transfer is minimal

$$E_f^{min} \approx \frac{\pi^2}{5\sqrt{2}} \frac{Q_f^2}{\eta} e^{-\frac{4\sqrt{2}}{3}\tilde{\sigma}_f\eta} E_*. \tag{A7}$$

This paper has been typeset from a TEX/ LATEX file prepared by the author.